Fraunhofer ENAS

CHEMNITZ UNIVERSITY OF TECHNOLOGY

Atomic Layer Deposition and Microanalysis of Ultrathin Layers

Marcel Melzer

October 17, 2011

of the Faculty of Natural Sciences
Chemnitz University of Technology

Bachelor Thesis

submitted to obtain the degree of

Bachelor of Science
(B.Sc.)

Examiner:	Prof. Dr. Stefan E. Schulz Fraunhofer ENAS Honorary Professorship "Technologien der Nanoelektronik" Faculty of Electrical Engineering and Information Technology Chemnitz University of Technology
Second Examiner:	Prof. Dr. Michael Hietschold Professorship "Analytik an Festkörperoberflächen" Faculty of Natural Sciences Chemnitz University of Technology
Supervisor:	Dr. Thomas Waechtler Fraunhofer ENAS Department "Back-end of Line"

Contents

List of Acronyms and Symbols

Acronyms

AFM	Atomic force microscopy
ALCVD	Atomic layer chemical vapor deposition
ALD	Atomic layer deposition
ALE	Atomic layer epitaxy
ALG	Atomic layer growth
BEOL	Back-end of line
CMOS	Complementary MOS
CNT	Carbon nanotube
CVD	Chemical vapor deposition
DFT	Density functional theory
DRAM	Dynamic random access memory
EDX	Energy-dispersive X-ray analysis
FTIR	Fourier transform infrared spectroscopy
GPC	Growth per cycle, i. e. film thickness increment per each complete ALD cycle
HOPG	Highly ordered pyrolytic graphite
IC	Integrated circuit
ILD	Inter layer dielectric
IR	Infrared
ITRS	International Technology Roadmap for Semiconductors
LDS	Liquid delivery system
MLE	Molecular layer epitaxy
MWCNT	Multi-walled carbon nanotube
NP	Nanoparticle
PEALD	Plasma-enhanced atomic layer deposition

sccm	Standard cubic centimeters per minute
SE	Spectroscopic ellipsometry
SEM	Scanning electron microscopy
SWCNT	Single-walled carbon nanotube
TEM	Transmission electron microscopy
TGA	Thermogravimetric analysis
XPS	X-ray photoelectron spectroscopy

Chemical Names

^{n}Bu	*n*-Butyl
acac	Acetylacetonate
hfac	Hexafluoroacetylacetonate
thd	Tetramethylheptanedionate
TMA	Trimethylaluminum

Symbols

λ	Wavelength
Ψ	Ellipsometric angle Psi
τ	Time constant (signal delay)
$\vec{a}_i$	Real space basis vector
$\vec{b}_i$	Reciprocal space basis vector
$\vec{C}$	Chiral vector
C_{coup}	Coupling capacitance between two adjacent metallization lines
d_t	Tube diameter
E	Energy
e	Elementary electric charge, $e = -1.602176565(35) \cdot 10^{-19}\text{C}$
E_g	Band gap energy
h	Planck constant, $h = 6.62606957(29) \cdot 10^{-34} J \cdot s$
p	Pressure
R_{metal}	Resistance of an interconnect line
T	Temperature

1 Introduction

Since their discovery in 1991 by Iijima[1], carbon nanotubes (CNT) have attracted the attention of many scientists [3]. The unique electrical, mechanical, optical and chemical properties make a whole range of promising applications thinkable, *e.g.* extremely small electron sources and transistors [4, 5]. However, up to the present CNTs are only used as AFM tips and in composite materials, *e.g.* to enhance the stiffness and the weight of high-end bicycle frames [6, 7]. Some applications of CNTs require the deposition of metals or other metal compounds on the CNTs. In the following, two examples for those metal decorated CNTs should be examined in more detail: the use in metallization systems of integrated circuits (IC) as conductive material and CNT-based sensor devices.

Due to their ballistic electron transport, CNTs are a highly promising material for future interconnects in ultra-large scale integrated (ULSI) ICs [8]. Ballistic transport means that the resistance of a CNT vanishes since no scattering of the electrons occurs and only a contact resistance between the CNTs and another conductive material is observed [9][2]. This is an advantage compared to the currently used copper, since the resistance R_{metal} of conductive copper paths will double within the next ten years, due to the increasing influence of scattering effects at interfaces and grain boundaries [11, p. 16]. This rising resistance R_{metal} causes an also increasing time delay τ, because these two properties are linked by:

$$\tau = R_{metal} C_{coup} \tag{1.1}$$

where C_{coup} is the coupling capacitance between adjacent conductive paths [12]. Therefore copper has to be replaced in specific areas of the metallization systems by new materials or technologies like superconductors, wireless or optical interconnects, metallic nanowires, nanoribbons or the already mentioned CNTs [13].

However, the currently used growth processes for CNTs cannot generate densities of nanotubes that are high enough to make nanotube interconnects competitive to copper based interconnects. Therefore, the connection of copper technology with the utilization of CNTs is highly promising for the realization of further technology nodes. This can be enabled either by the decoration of the CNTs with metallic nanoparticles (NP), which influence the electronic properties of the CNTs, or the deposition of a conformal Cu layer on the CNTs and the subsequent closing of the space between the CNTs by electrochemical deposition (ECD) [11, p. 137] [14, 15].

[1] The first indication of the existence of CNTs were TEM pictures published by L. V. Radushkevich and V. M. Lukyanovich in the Soviet Journal of Physical Chemistry in 1952 [1]. Nevertheless, this paper remained extensively unknown in the scientific world, because it was only published in Russian. Therefore many people claim the article of Iijima in 1991 as the discovery of CNTs [2].

[2] For a more detailed description of the electron transport in CNTs which takes transmission probabilities and localization effects in account see [10, p. 137-162].

A further potential application of CNTs are gas sensors that are based on the sensitivity of semiconducting CNTs towards the adsorption of molecules [17]. Nevertheless, sensors that are based on pure CNTs are only sensitive to gases that bind to the CNTs and for which charge transfer between the molecule and the CNT occurs. For example, the toxic gas CO cannot be detected with pristine CNTs since it does not interact with the surface of the CNT [17]. Therefore, the CNTs have to be decorated with NPs that are sensitive to the gas that should be detected [18]. For a CO sensor CuO seems to be an appropriate functionalization material [19].

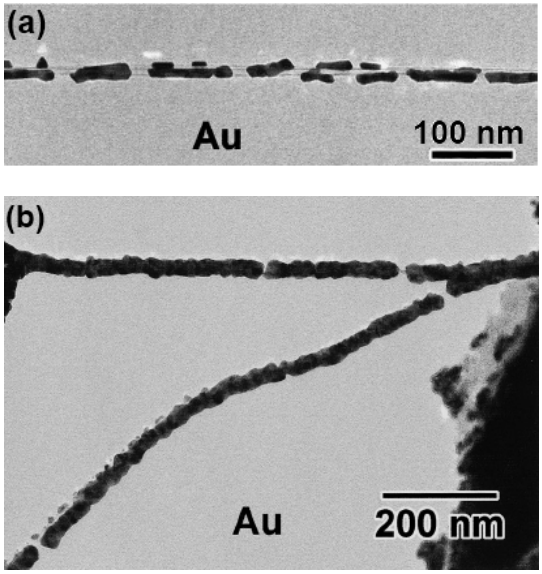

Figure 1.1: Electron microscope images of (a) pristine CNTs and (b) with X-100 Triton pretreated CNTs. Both CNTs were coated with Au by electron-beam evaporation [16].

These two examples make clear that the deposition of metal or metal compounds on CNTs is necessary for different potential applications of CNTs. However, the growth of films on CNTs is challenging due to various reasons. An appropriate deposition method has to be applied, which is able to uniformly coat the CNTs with their high aspect ratio. Therefore atomic layer deposition (ALD) is probably the most promising approach. However, out of the numerous known copper and copper compound ALD processes a convenient one has to be chosen. It is known that the surface of CNTs and the related graphite is chemically relatively inert, due to the stable sp^2-hybridization of the carbon atoms [20]. Hence, it is necessary to functionalize the CNTs by different treatments before the ALD to obtain the desired deposition characteristics, see Fig. 1.1. A pretreatment has to be chosen that is appropriate for the integration into the fabrication of metallization systems.

The following *chapter 2* starts with a basic introduction of ALD. After a discussion of several ALD processes, a Cu_xO process was chosen for this thesis, which relies on a Cu(I) β-diketonate precursor. *Chapter 3* characterizes the properties of CNTs as well as different synthesis methods. Additionally, *chapter 3* contains a subsection about surface chemistry of CNTs and a survey of different possible processes to functionalize the surface of CNTs and make them accessible for ALD. Based on this comparison a functionalization of the CNTs with water vapor, oxygen and wet oxygen was chosen to be examined within this work. *Chapter 4* presents the equipment for the copper oxide ALD and the functionalization as well as the analytical methods. Besides this, the formation of the used test structure is described, likewise the applied ALD process. *Chapter 5* shows the results of the analysis of the Cu_xO coated CNTs and the ellipsometry measurements of SiO_2 substrates, which were used to monitor the ALD process. The thesis is completed in *chapter 6* with a summary and an outlook.

2 Atomic Layer Deposition

2.1 Introduction

Atomic layer deposition is a thin film deposition technique and is very familiar to chemical vapor deposition (CVD) processes. In contrast to a CVD process, the reaction partners are introduced separately into the process chamber, which allows the usage of highly reactive reaction partners as well as conformal deposition characteristics due to the self-limiting chemical surface reactions. Investigations of the basic principles of ALD were already carried out in the 1960s in the former Sowjet Union [21]. Independently of the Russian scientist ALD was also investigated by a Finish group around T. Suntola who applied for a patent in 1977 on atomic layer epitaxy of compound thin films [22] [1].

The first application of ALD was the deposition of TiO_2 , Al_2O_3 and doped ZnS for the use in thin film electroluminescent displays [23]. In the last years ALD has been gaining more and more attention due to the continuous downscaling in microelectronics and the need for conformal and void-free thin films in structures with high aspect ratios. High-κ dielectrics (HfO_2, ZrO_2) for CMOS and DRAM technology are already deposited via ALD [24]. Furthermore, ALD metals and nitrides are probably going to be implemented as seed layers as well as diffusion barriers for Cu metallization [25].

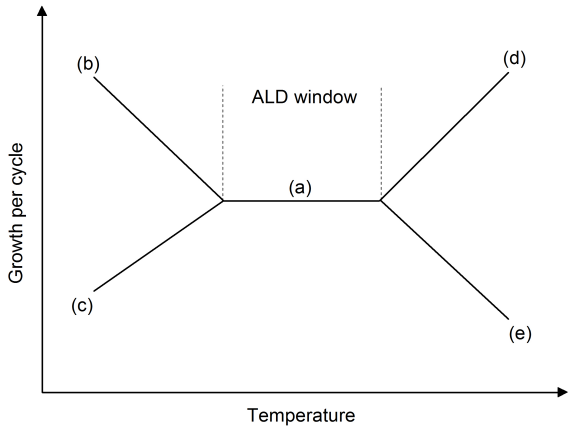

Figure 2.1: The ALD processing window (a) is limited due to precursor condensation (b), incomplete reactions (c), precursor decomposition (d), and precursor desorption (e).

[1] Besides the already mentioned terms ALD and ALE further names are in use like atomic layer growth (ALG), atomic layer chemical vapor deposition (ALCVD), molecular layer epitaxy (MLE) etc. [23]

2.2 Basic Principles and Features of ALD

ALD is a cyclic process consisting in the most simple case of 4 steps: (I) exposure of the first reactant, (II) purge or evacuation of the reactor, (III) exposure of the second reactant and (IV) purge or evacuation of the reactor. ALD processes including more than two reactants require additional steps. The reactant inserted during step 1 and 3 into the process chamber react/chemisorb only with specific surface groups [26]. Therefore the growth per cycle (GPC) is limited by these saturation characteristics[2]. The ideal ALD process can only be carried out in an appropriate temperature range, the so called ALD window, see Fig. 2.1 [27]. Due to the self-limiting character of the growth process and the separate insertion of the reactants, ALD has some advantages like [23]:

- accurate and simple thickness control by the number of cycles
- less need of precursor flux homogeneity compared to CVD processes $\rightarrow$ large-area and large-batch capability
- high conformality (coating of porous material or substrate with high aspect ratios)
- lower processing temperatures than CVD processes

But also the disadvantages should be mentioned here:

- low deposition rates
- lack of industry-suitable ALD processes for important materials, like for example SiO_2 or TaN

2.3 Chemisorption Mechanisms

Due to the important role of surface reactions for ALD they are treated here a little more detailed. Generally three classes of chemisorption mechanisms are responsible for the self-limited reactions during ALD: ligand exchange, dissociation and association [28], see Fig. 2.2. Ligand exchange occurs if the precursor molecule is split up and a fragment of it forms volatile species with surface groups. In contrast, dissociation appears if the fragment of the precursor remains at the surface via chemisorption at surface groups. The adsorption of the whole precursor molecule is called association.

For those reactions surface groups are needed. For example, the well understood ALD process of trimethylaluminium (TMA) with H_2O as co-reactant towards Al_2O_3 requires OH groups or oxygen bridges of silica as reactive groups [28]. Experiments have shown that the amount of deposited Al_2O_3 is linear proportional to the OH surface concentration [29].

2.4 ALD of Copper and Copper Compounds

Various experiments of Cu ALD process have shown that a deposition of metallic copper is only possible by reducing the precursor [30]. One approach is the application of atomic hydrogen within a PEALD process [31, 32]. Nevertheless, the application of a plasma is not suitable for the coating of CNTs, which are positioned in vias with high aspect ratio, which are typical for metallization systems. The reason for this is the depletion of the hydrogen plasma in deep trenches due to recombination. This would cause nonuniform coating of the CNTs.

[2] Due to the interaction of the substrate and the ALD film, the GPC can depend on the number of cycles. Three cases can appear: substrate-enhanced growth, linear growth, substrate-inhibited growth [12].

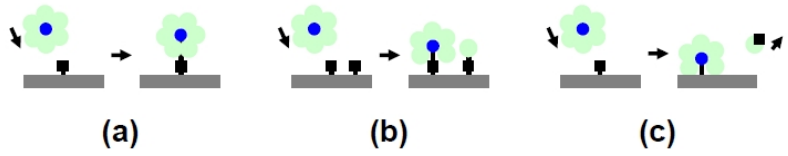

Figure 2.2: Mechanisms of chemisorption which are relevant to ALD: (a) association, (b) dissociation, (c) ligand exchange [12].

A thermal ALD process which uses [CuCl] as precursor requires high processing temperatures between 375 and 475°C [33]. Depending on the substrate, the Cu layer agglomerates due to the high process temperature [34]. Therefore, this process is probably not able to deposit a conformal Cu layer on CNTs. Additionally, the high processing temperatures in connection with the co-reactants water or hydrogen could eventually destroy the vertical alignment of the CNTs [35].

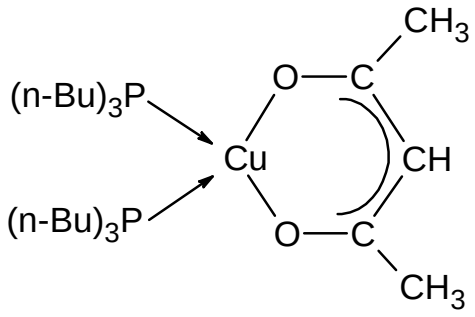

Figure 2.3: Structure of $[(^{n}Bu_3P)_2Cu(acac)]$. The precursor is liquid under standard conditions, showing a pale-yellow color [12].

The metalorganic precursor copper(II) hexafluoroacetylacetonate, $[Cu(hfac)_2]$, requires a minimal processing temperature of 230°C [36]. Nevertheless, precursors which contain fluorine mostly form layers with low adhesion, due to the accumulation of fluorine-containing residues at the interface to the substrate [37]. However, the application of the fluorine-free copper(II) tetramethylheptanedionate, $[Cu(thd)_2]$, is also not suitable for the ALD on CNTs, because this ALD process depends strongly on the interaction of the precursor with a catalytic substrate like Pt or Pd [38].

Further possible precursors for Cu ALD are Cu(I) amidinates [39, 40]. Their outstanding feature is a processing temperature below 200°C. However, those precursors are unpractical, because they are solids under standard conditions.

Due to the challenges for the direct ALD of metallic Cu, the deposition of copper compounds such as nitrides and oxides has been examined [12, p. 56-57]. These compounds can be reduced subsequently to metallic copper. For the investigation of the ALD characteristic on CNTs, a process which belongs to this group and deposits Cu_xO was chosen [12]. This process relies on the Cu(I) β-diketonate precursor bis(tri-*n*-butylphospane)copper(I)acetylacetonate, $[(^{n}Bu_3P)_2Cu(acac)]$, see Fig. 2.3. The advantages of this thermal ALD process are the straightforward and inexpensive precursor synthesis. The precursor is liquid under standard conditions and it is fluorine free. This is expected to improve the adhesion compared to fluorine-containing precursors. Furthermore, the process temperatures are low ($T \leq 160$ °C). The ALD process is described more detailed in *chapter 4*.

3 Carbon Nanotubes

3.1 Chemical Bonds in Carbon Structures

There are several allotropes of carbon, e.g. graphite, diamond, buckyballs and CNTs. Depending on the number of shells one can distinguish between single-walled carbon nanotubes (SWCNTs) and multi-walled carbon nanotubes (MWCNTs). This diversity of carbon allotropes has its seed in the possibility of carbon to form different hybridization states of its 4 valence electrons, see Fig. 3.1. These hybridization states are called sp^n-hybridization, because they arise from a linear combination of one s- and n p-electrons. This hybridization leads to the formation of (n+1) σ-electrons (the sp^n hybridized states) whose clubbed atomic orbital determines the local atomic structure. If sp^2-hybridization occurs besides the 3 sp^2-states a π-electron is generated. The interaction of those π-electrons causes the cohesion of neighboring graphite layers in graphite and neighboring tubes in MWCNTs [41, p. 10-11].

$$C \quad \underset{1s}{\uparrow\downarrow}\ \underset{2s}{\uparrow\downarrow}\ \underset{2p_x}{\uparrow}\ \underset{2p_y}{\uparrow}\ \underset{2p_z}{} \qquad C_{sp^2} \quad \underset{1s}{\uparrow\downarrow}\ \underset{sp^2}{\uparrow}\ \underset{sp^2}{\uparrow}\ \underset{sp^2}{\uparrow}\ \underset{2p}{\uparrow} \qquad C_{sp^3} \quad \underset{1s}{\uparrow\downarrow}\ \underset{sp^3}{\uparrow}\ \underset{sp^3}{\uparrow}\ \underset{sp^3}{\uparrow}\ \underset{sp^3}{\uparrow}$$

Figure 3.1: The ground state of carbon and two different hybridization states, the sp^n-states form σ-electrons and the p-state of the sp^2-hybridization generates a π-electron, see text.

3.2 Structure of Carbon Nanotubes

SWCNTs can be described as rolled-up sheets of graphene. To set the way in which the SWCNTs can be formed out of the graphene plane and to determine the properties of the CNTs the chiral vector $\vec{C}$ is introduced. This vector $\vec{C}$ connects two carbon atoms of the graphene plane that overlap after the rolling up process, see Fig. 3.2. The chiral vector $\vec{C}$ can be described as linear combination of the two basis vectors $\vec{a}_1$ and $\vec{a}_2$:

$$\vec{C} = \mathrm{n}\vec{a}_1 + \mathrm{m}\vec{a}_2 = (n,m) \qquad (0 \leq m \leq n;\ m,n \in \mathbb{N}) \tag{3.1}$$

Not every chirality (n, m) is observed, because if the nanotube becomes smaller, the strain energy increases due to stronger curvature. This makes the rolling up of the graphene layer energetically inappropriate [43, p. 139]. Therefore, SWCNTs have typically a diameter larger than 1 nm. SWCNTs with a diameter bigger than 4 nm are usually not observed because larger SWCNTs collapse if they are not stabilized with other shells [11, p. 27-28].

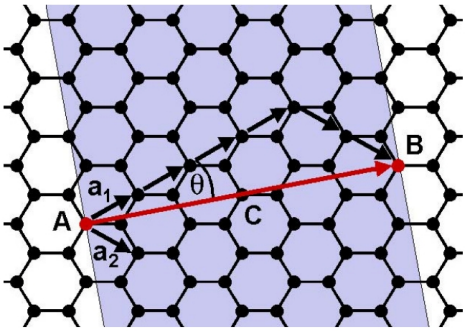

Figure 3.2: Structure of a graphite lattice, the unit vectors $\vec{a}_1$, $\vec{a}_2$; the chirality vector $\vec{C}$ and the chirality angle Θ are plotted. If the graphite sheet is rolled up and point A and B are getting connected, a (4,2) SWCNT is formed. [42, p. 7]

The distance between two shells of MWCNTs is in the range of 0.344 to 0.36 nm [44]. Among the classification into SWCNTs and MWCNTs single-walled CNTs are divided into three subgroups: zig-zag SWCNTs are characterized by $n = m$, armchair CNTs by $m = 0$ and all other SWCNTs are just called chiral SWCNTs.

As already mentioned above the properties of a SWCNT are determined by the chirality vector $\vec{C}$. One example for it is the energy gap of the SWCNTs. CNTs for which the difference between n and m can be divided by three have no bandgap and are therefore metallic[1]. All other CNTs are semiconducting with a bandgap which is inversely proportional to the tube diameter d_t ($E_g = 0.41$ eV/d_t[nm]) [45].

3.3 Synthesis of Carbon Nanotubes

There are three main methods for the production of CNTs, arc discharge, laser ablation and chemical vapor deposition (CVD). Arc discharge and laser ablation rely both on the evaporation of graphite either by a vacuum arc discharge or by a laser beam [47, 48]. When the so gained elemental carbon hits any surface in the process chamber, it can redeposit and form different allotropes of carbon including CNTs. Experiments have shown that SWCNTs are only formed if the graphite which is evaporated contains catalytic metals like Co, Ni, Fe, Y or Gd [49–51].

[1] It is found that in some cases there is a small bandgap ($E_g \leq 0.06$eV/d_t^2[nm]) even if $n - m$ is divisible by 3 [45]. Those CNTs are called semi-metallic. It can be shown that only armchair CNTs with $n = m$ are truly metallic [46]

The basic principle of the third method to form CNTs (CVD) is the catalytic decomposition of a carbon containing material (C_2H_2, C_2H_4, CH_4, CO) on transition-metal nanoparticles (Fe, Co, Ni) [52–54][2]. Due to the usually lower process temperatures, CNTs which are produced via this approach contain more defects than CNTs formed by the methods mentioned above. Nevertheless, CVD makes it possible to grow CNTs in a large scale, area selective. The CNTs used for this thesis were also prepared by CVD. The used CNT growth process is described in *chapter 4*.

CNTs can be purified after the synthesis e.g. by treatment with nitric acid or thermal oxidation with oxygen to remove unwanted byproducts of the fabrication like amorphous carbon and buckyballs [56].

3.4 Surface Chemistry of Carbon Nanotubes

The sp^2-hybridization of the carbon nanotubes makes them in chemical terms relatively inert. Therefore, it necessary to use aggressive reactants like fluorine or ozone at elevated temperatures to enable a covalent bond between the carbon atoms of the CNT and the adsorbed molecule [57]. It should be mentioned here that in general CNTs with a small diameter are more reactive due to the strong curvature [57], because this curvature disturbs the plane structure of the sp^2 hybridization. Covalent sidewall functionalization can strongly disturb the structure of the CNTs [57]. The pretreatment of CNTs with fluorine or ozone, which is described in the next section, can be classified to this group.

In contrast, defect-group chemistry relies on the coupling of molecules to already existing defect sites of the CNT. Defects of CNTs are buckyball-like end caps, pentagon-heptagon pairs and vacancies. Approx. 5% of the carbon atoms of a CNT are localized at defects [58]. Furthermore, experiments indicate that a limited number of defects does not influence the properties of CNTs [59]. The defects are often occupied with carbonyl groups which can be used as anchor groups for other molecules [59]. These carbonyl groups are mostly introduced to the CNTs during the purification with different oxidation agents. The oxidation of CNTs with air, oxygen or nitric acid which are described more detailed in the next section are examples for defect-group chemistry.

The sp^2-hybridization can also be taken as advantage by using functionalization reactants which exhibit big π-electron systems. For example, the aromatic groups of several organic molecules couple to the CNTs due to the interaction of the π-electrons of the benzene rings and the π electrons of the CNTs [60]. In contrast, the adsorption of non-aromatic long-chain organic molecules like sodium dodecyl sulfate (SDS) is probably caused by weaker Van der Waals forces [61]. Those functionalizations are for example used to make the CNTs soluble in water or ethanol [43, p. 142-143]. The functionalization of CNTs with a physisorbed NO_2 layer can be classified to this group of weakly bonded functionalizations.

[2] Besides the mainly used CVD growth by NPs which contain transition metals there are also approaches which are based on non-transition metals, ceramic and semiconducting NPs and also on graphite substrates without NPs, see [55]

3.5 Functionalization of CNTs for ALD

This section gives a literature survey of functionalizations that have already been used to perform ALD on CNTs or on graphite. Besides this, further possible functionalization are described, which introduce reactive groups to the CNTs, see Tab. 3.1. There are many reviews on the surface chemistry and the functionalization of CNTs, but most of the approaches mentioned there are not applicable in the fabrication of ICs due to the reasons listed below [57, 59, 62–64].

Because of their chemical inertness, CNTs require a chemical modification of their surface to enable chemisorption of the ALD precursor on reactive groups [65]. It is generally known that hydroxyl groups play an important role for the deposition of oxide films by ALD [66, 67]. Maybe also oxygen embedded into the structure of the CNTs can be reactive towards the precursor [68]. However, due to the lack of knowledge about the reaction mechanisms of the Cu_xO ALD process used in this thesis, it is not known which reactive groups are reactive towards the applied precursor. The functionalization should fulfill following requirements to be capable of being integrated into the production of interconnect systems with high aspect ratios:

- in situ process
- process temperatures below 450°C (Back-end-of-line [BEOL] limit)
- thermal process, no plasma enhancement
- no destruction of the vertical alignment of the CNTs

It was recently shown that a conformal Al_2O_3 ALD layer can be deposited on CNTs which were functionalized by adsorption of NO_2[69]. Due to the weak bond of the NO_2 to the CNTs the functionalization layer has to be stabilized by altering exposure of NO_2 and the Al_2O_3 precursor trimethylaluminium (TMA) at ambient temperature. Like the ALD process this treatment is self limiting, because the NO_2 adsorbs only on the pristine CNT surface and the TMA adsorbs only at areas where already NO_2 has been adsorbed. Therefore a system of one monolayer NO_2 followed by a monolayer TMA is achieved [70]. Afterwards the temperature is increased to the normal process temperature and the ALD process is carried out. The big advantage of this method is that the adsorption of NO_2 does not depend on defects of the CNTs because it is physorbed by van der Waals forces. Therefore the functionalization occurs on the whole CNT and not only on defect sites. The disadvantage of this method is the low adhesion of the functionalization layer and the deposited Al_2O_3 on the CNTs. TEM images have shown that the ALD film can slide off the ends of the CNTs leaving bare ends.

Ammonia also physisorbs on CNTs but only at temperatures below 140 K. Above this temperature ammonia chemisorbed at defect sites only remains on the CNT up to 250°C [71, 72].

The treatment of CNTs with nitric acid or a mixture of nitric and sulfuric acid at temperatures near the boiling point of the used acid mixture (120-140°C) is a further approach for the functionalization of CNTs [73, 74]. The reaction of the acid with the CNTs generates OH groups at defects on the CNTs. Furthermore new defect sides are generated [59]. The density of attached hydroxyl groups can be tuned by the duration of the acid treatment [75]. However, this method is unpractical due to the danger that comes from boiling acid, filtration and washing steps that are required to recover the CNTs from the acid mixture and the problems with the vertical aligned placement of the functionalized CNTs in metallization structures. Those problems can be avoided using gaseous nitric acid as it has been reported by Xia et al. [76].

ALD experiments on graphite substrates have shown that Al_2O_3 deposition occurs only on step edges of the graphite. Via a pretreatment with O_3, deposition also occurs on the graphite planes [20]. Additional to this, Fourier transform infrared spectroscopy (FTIR) analysis revealed that oxygen groups on the surface of SWCNTs, which had been exposed to O_3 at ambient temperature, are stable up to a temperature of about 200°C [77].

Various plasma gases were used such as oxygen, ammonia or tetrafluoromethane to create different surface groups on CNTs [78–84]. Furthermore, Hossbach et al. have shown that MWCNTs can be coated conformaly with Ta_2CN via a PEALD process which uses a hydrogen plasma as reducing agent [85].

There are many papers that describe thermal oxidation with air, water or oxygen as a tool for gas phase purification of CNTs due to the fact that the oxidation is more aggressive to amorphous carbon than to CNTs [86–89]. During this treatment also functional groups like -OH or -O are introduced to the surface of the CNTs. Those reactive groups can be used as a starting point for ALD. Nevertheless, those processes are mostly carried out in pressure and temperature ranges that are too high for the application in IC fabrication. An exception is the paper of Bu et al. [35], were a purification process using oxygen is examined in the temperature range from 300 to 450 °C at a pressure of 2 mbar . This method preserves the vertical alignment of the CNTs up to a temperature of 300°C. DFT calculations of the interaction of oxygen and water with SWCNTs by Da Silva et al. have shown that an oxidation of the CNTs with a mixture of oxygen and water is favorable compared to the two reactants alone [90]. Due to the straightforwardness of this pretreatment as well as the preservation of the vertical alignment of the CNTs with proper process parameters the effect of a thermal oxidation via water vapor, oxygen and wet oxygen is examined within this thesis. Furthermore, the use of these gases enables an in-situ functionalization of the CNTs and a subsequent ALD without breaking the vacuum.

It should also be mentioned here, that the introduction of new defect sites via an Ar plasma can enhance the functionalizations mentioned above which require dangling bonds on the CNT surface [82, 84]. A further approach for the functionalization of CNTs is the substitution of carbon by fluorine. To achieve this different pretreatments are possible, such as the above mentioned plasma process. Additional approaches are either thermally or UV induced [91, 92].

Table 3.1: Examples for functionalization of carbon materials

	Treated with	Added group	Phase	Temperature	Duration	Growth mode	Tested on	Notes	Reference
already tested pretreatment for ALD	O_2/Ar	-O	plasma	-	<1h	NP	MWCNTs	- tested for Pt ALD - density of NPs can be tuned	[78–80]
	H_2/Ar	-	plasma	-	<1 h	conformal layer	MWCNTs	- tested for PEALD of Ta_2CN	[85]
	NO_2	-NO_2	gas	25°C	<1 h	conformal layer	MWCNTs SWCNTs	- low adhesion - tested for Al_2O_3	[69, 70]
	O_3	-O	gas	200°C	<1 h	layer	HOPG	- tested with TMA/O_3 ALD	[20]
	HNO_3 H_2SO_4	-OH	liquid	120-140°C	>18 h	NP	MWCNTs SWCNTs	-washing and drying steps - tested for ZnO - density of NPs can be tuned	[59, 73–75]
possible pretreatment for ALD	HNO_3	-OH	gas	120-250°C	7-17 h	-	MWCNTs	- probably similar to the pretreatment with liquid HNO_3	[76]
	O_2	-O	gas	300-450°C	<1 h	-	MWCNTs	- above 300°C destruction of the vertical alignment	[35]
	NH_3	-	gas	25°C	<1 h	-	MWCNTs SWNCTS	- chemisorption at defect sites	[71, 72]
pretreatment for further functionalization	Ar	defect sites	plasma	-	<1 h	-	MWCNTs	- defect sites have higher reactivity	[82, 84]
	F_2	-F	gas	150-250°C	5 h	-	MWCNTs SWCNTs	- CNTs become non-conductive if CF_x, x > 0,5 - thermal, UV or plasma process	[91, 92]

4 Experimental

4.1 Sample Preparation

To investigate the effect of thermal oxidation of CNTs on a subsequent Cu_xO ALD for an application of the CNTs in metallization systems a test vehicle was used that should reflect the situation in interconnect structures. Therefore the layer stack shown in Fig. 4.1 was processed by deposition, photolithography and different etching steps to form vias with a Ni/Ta layer stack at the bottom. To start the transition of the Ni layer towards Ni NPs the substrate was heated within 45 minutes to 606°C under a H_2/N_2 atmosphere (p = 700 mbar). The interaction of the Ta layer with the Ni NPs causes later vertically aligned growth of CNTs inside the vias. Outside the vias no growth occurs due to the interaction of Ni and W. After the heating up, the temperature was maintained constant at 606°C for 10 minutes. Subsequently the atmosphere in the process chamber was changed by adding C_2H_4, which causes CNT growth. Besides this, the process pressure was lowered to 200 mbar. After 10 min the growth process was stopped by turning off the C_2H_4 and the H_2. After 5 min more at 606°C the process was finished by cooling down the samples in a N_2 atmosphere.

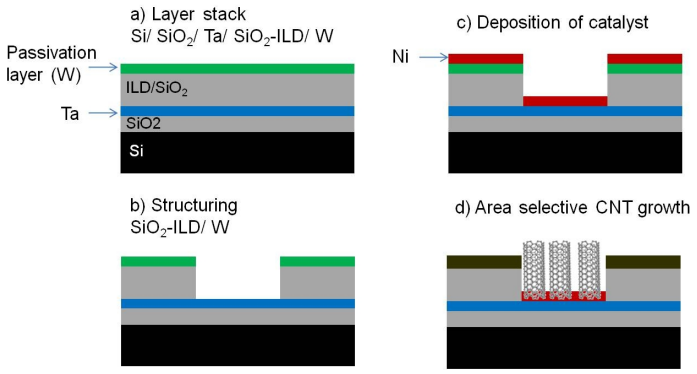

Figure 4.1: Fabrication steps of the CNT samples embedded in via structures

4.2 ALD Equipment

The ALD and the thermal oxidation were carried out in a cold-wall reactor which is able to handle wafers up to a size of 4 inch in diameter. This research tool is equipped with a load-lock chamber, a resistive heating, a turbo pump and a roots pump. During the ALD process, the pressure in the reactor is controlled via a butterfly valve between the process chamber and the roots pump. To provide the

necessary gases for different ALD and reducing processes, the ALD system is furthermore equipped with two bubbler systems for the supply of water vapor and formic acid as well as gas pipelines for O_2, N_2, Ar, H_2 and NH_3. The flux of the gases is controlled via mass flow controllers (MFC). The Cu(I) β-diketonate precursor applied for this thesis is liquid under standard conditions and therefore it is evaporated via a liquid delivery system (LDS). The whole tool is more detailed described in [12].

4.3 Oxidation of the Carbon Nanotubes

To investigate the influence of different thermal oxidations on the subsequent Cu_xO ALD, CNT-samples were heated to 100, 200, 300°C. At this the temperatures the CNTs were exposed to oxygen, water vapor or wet oxygen (H_2O+O_2) for 30 min at a pressure of 1.3 mbar, see Tab. 4.1. A maximum temperature of 300°C was chosen to avoid the loss of the vertical alignement of the CNTs [35].

Table 4.1: Process gases used for the different thermal oxidations.

Oxidizing agent	**Process gases**
H_2O	18-20 mg/min H_2O 210 sccm Ar carrier gas
O_2	45 sccm O_2 210 sccm Ar
H_2O+O_2	18-20 mg/min H_2O 45 sccm O_2 210 sccm Ar carrier gas

4.4 Atomic Layer Deposition

As already mentioned in *chapter 2*, an ALD process was chosen for the investigations within this thesis, which relies on the Cu(I) β-diketonate precursor, $[(^nBu_3P)_2Cu(acac)]$. Wet oxygen was used for the oxidation of the precursor, because in the reference it is reported, that this enables the formation of a closed layer Cu_xO on various substrates [12, p. 72-78]. The ALD window of this process as well as the GPC and the film morphology depends on the used substrate, see Tab. 4.2.

For the investigations within this thesis a process temperature of 135°C was used. This temperature value is slightly above the ALD window, which causes a higher GPC, due to the beginning CVD growth above 130 °C [12, p. 72-78]. This was accepted, because with a higher GPC 400 ALD cycles deposit enough Cu_xO for the subsequent characterization of the samples. Futhermore, the film morphology is not influenced by the higher temperature [12, p. 72-78]. 600 ALD cycles would have been necessary at a temperature within the ALD window. This higher number of cycles would have consumed the limited amount of precursor faster and therefore it would not have been possible to prepare all samples with the same precursor batch. Inhomogeneities due to the beginning CVD growth can be neglect because of the small size of the used samples. The process parameters are shown in Tab. 4.3.

Table 4.2: ALD characteristics using $[(^{n}Bu_3P)_2Cu(acac)]$ and wet oxygen on various substrates [12, p. 147].

	Substrate			
	Ta	**TaN**	**Ru**	**SiO_2**
ALD window [°C]	115-125	115-125	100-120	110-120
GPC in the ALD window [Å]	0.12-0.14	0.08-0.09	0.13-0.15	0,05 (wet SiO_2) 0.12 (dry SiO_2)
Film morphology	Smooth, continuous films after island coalescence	Continuous films with isolated clusters	Smooth, continuous films replicating substrate roughness	Continuous films smoothening the substrate

During the ALD process mainly Cu_2O is deposited. The ALD film contains impurities such as C (2-3 %), Cl (0.2-1.2 %) and P ($\leq$2 %) as well as CuO and $Cu(OH)_2$ at the surface due to the exposition to air after the ALD.

Table 4.3: ALD cycle for the deposition of Cu_xO.

Step	**Pulse length (s)**	**Process gases**
1 – Precursor exposure	4	10-20 mg/min precursor 740 sccm Ar carrier gas
2 – Purging step	5	145 sccm Ar
3 – Oxidation	8	18-20 mg/min H_2O 45 sccm O_2 355 sccm Ar carrier gas
4 – Purging step	5	145 sccm Ar

4.5 Methods for Characterization

Transmission Electron Microscopy was used to obtain high-resolution images of the CNTs and area selective electron diffraction images of the CNT samples. These characterizations were carried out with a Philips CM20FEG 200keV TEM. The samples for the TEM analysis were prepared by scratching TEM-grids over the CNT samples.

Raman spectroscopy is a powerful tool to determine the properties of CNTs. Raman measurements rely on the the energy difference between incident light and scattered light. This energy difference is the so called Raman shift and it allows conclusions from the properties of the sample such as composition and crystallinity [93]. One of the main features (D-band around 1350 cm^{-1}) of a typical Raman spectrum of CNTs is proportional to effects which lower the crystalline symmetry like vacancies or impurity atoms. In combination with the defect independent G-band (around 1600 cm^{-1}) this makes it possible to determine the crystallinity of the CNTs by the ratio of the the intensities of these two peaks

I_D/I_G [94–96]. Measurements were performed with a Horiba Scientific LabRAM HR and two different light sources, a green ($\lambda = 514$ nm) and a UV laser ($\lambda = 325$ nm). For comparison the Raman spectra were smoothed via a FFT filter and normalized to the G-band.

Scanning Electron Microscopy was applied to obtain structural information of the CNTs. For this purpose a Zeiss Auriga 60 and a Zeiss Supra 60 were used. The basic principle of a SEM remains on the detection of secondary or primary electrons from the surface of the sample. Those electrons are produced by rastering an electron beam with an energy of 1 keV over the sample. To analyze the effect of the different treatments onto CNTs in vias the samples were split to gain cross sectional images.

Energy dispersive X-ray spectroscopy (EDX) was performed with EDX systems (Bruker X-Flash 5030, 5010 respectively) attached to the SEM tools mentioned above. EDX allows to identify the material configuration of a sample by exiting the atoms in the sample via the electron beam of the SEM. When the exited atoms relax into a lower state, X-ray photons with characteristic energies are emitted. In contrast to the SEM analysis, EDX measurements where not carried out on cross sections of the samples but perpendicular to the surface. This secures that always the same amount of CNTs is exited by the electron beam. At cross section this would not be possible, because it cannot be guaranteed, that the fraction of the cross sections proceeds parallel to the via rows. For comparison the EDX spectra were normalized to the C-peak to exclude the influence of the density of CNTs which depends slightly on the position on the wafer.

Spectroscopic ellipsometry (SE) is a nondestructive optical method for the investigation of the dielectric properties and the thickness of thin layers and layer stacks. This characterization technique measures the phase shift Δ and the polarization angle Ψ of a light wave reflected at the sample. Ellipsometry was applied to monitor the ALD. Therefore besides the CNT samples always a SiO_2 substrate was placed in the reactor which was analyzed afterwards via ellipsometry. For these analyses a SENTECH SE 850 spectroscopic ellipsometer was used together with the software SpectraRay 2. The investigations were performed in the wavelength range from 190 to 830 nm for the angles 60°, 65° and 70°. For the modeling of the SiO_2 layer a Cauchy Model was applied. To take the stronger absorption of the Cu_xO into account a Lorentz-Drude model was used for the fitting of this layer. A more detailed description of the used models as well as general information about SE can be found in [12].

5 Results

5.1 Electron Microscopy

The following section deals with the analysis of the CNT samples by electron microscopy. An overview of all samples is compiled in Fig. 5.2. This figure should be the first point of reference. The text refers to more detailed images of the samples on the pages.

The comparison of pristine CNTs with Cu_xO coated CNTs and without any pretreatment indicates a slight increase of the diameter of the CNTs, see Fig. 5.3. The thickening seems to be uniform from the via bottom to the top of the CNTs. The CNTs which were oxidized at 100 and 200°C show an analog behavior in the SEM, independently of the oxidation agent. TEM images suggest that this thickening is caused by the deposition of Cu_xO NPs that are too small to be resolved by the SEM, see Fig. 5.1 (a)-(b). Potentially also charging effects of those NPs play a role. In the case of the sample which was not oxidized before the ALD process, no NPs are visible in the TEM image, see Fig. 5.1 (c). It seems like the deposition of Cu_xO occurs only on small parts of the CNTs and thereby a rather layer-like growth occurs. SEM images of samples after pretreatments with various oxidation agents exhibit the formation of bigger Cu_xO NPs on the samples which were oxidized at a temperature of 300°C, see Fig. 5.4, 5.5 and 5.6. However, the NPs which were formed on the sample which was oxidized with wet oxygen at 300°C are less sharply separated from the CNTs than NPs which can be seen on the two other samples oxidized at 300°C .

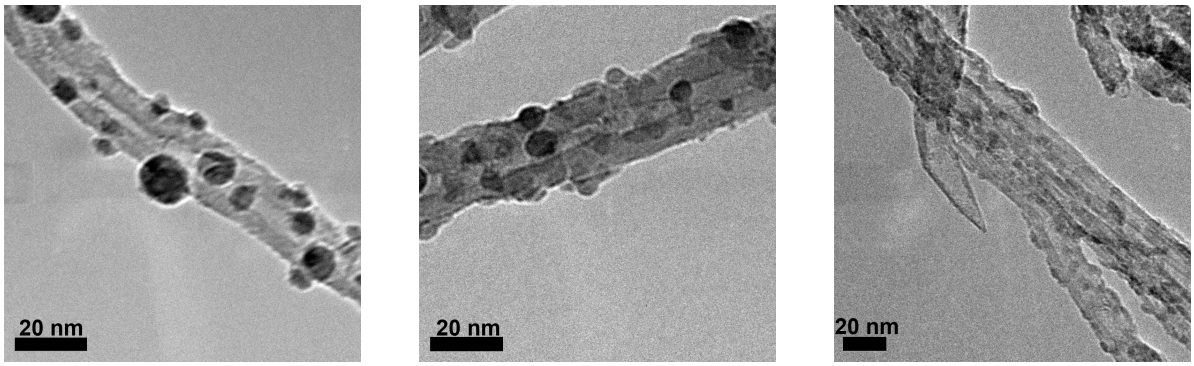

(a) 100°C H_2O+O_2 + ALD (b) 200°C H_2O+O_2 + ALD (c) unpretreated CNTs + ALD

Figure 5.1: Images (a) and (b) indicate the formation of NPs. It is expected that the other samples which were oxidized below 300°C show a similar surface morphology, independently of the used oxidation agent. In contrast, on the sample which was not oxidized before the ALD no NPs are visible.

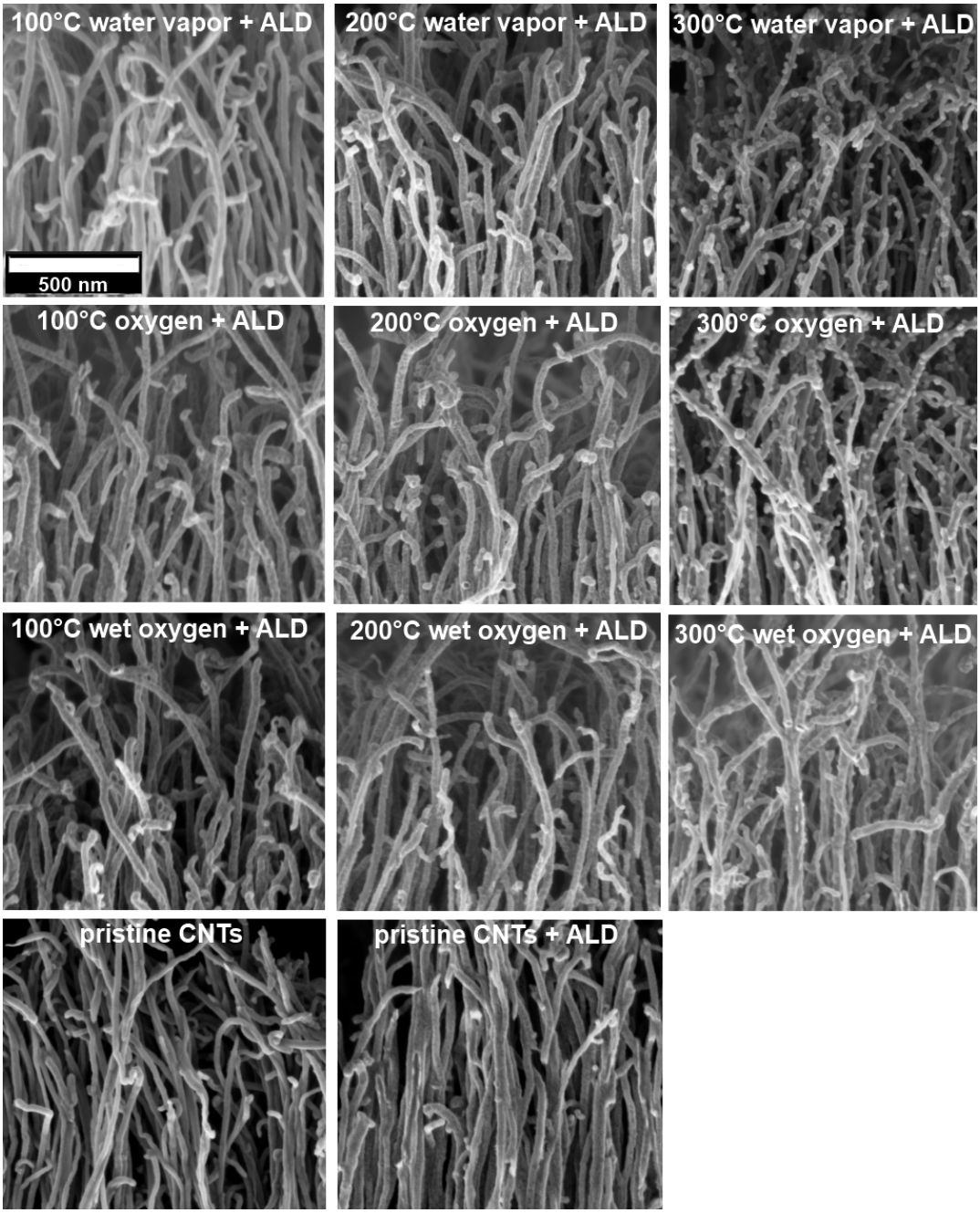

Figure 5.2: SEM image overview of all MWCNT samples. The comparison of pristine CNTs with pristine CNTs after ALD shows a slight thickening of the CNTs. NPs can be seen at samples that were pretreated at 300°C, independently of the oxidation agent. If the oxidation temperature is lower than 300°C, then the NPs are probably smaller and can only be resolved in the TEM, see Fig. 5.1 (a, b). At the sample which was oxidized with wet oxygen at 300°C the NPs are less sharp compared to the other pretreatments at 300°C. This can be possibly attributed to the partial destruction of the CNT sidewall, see text. The scale bar of 500 nm applies to all images.

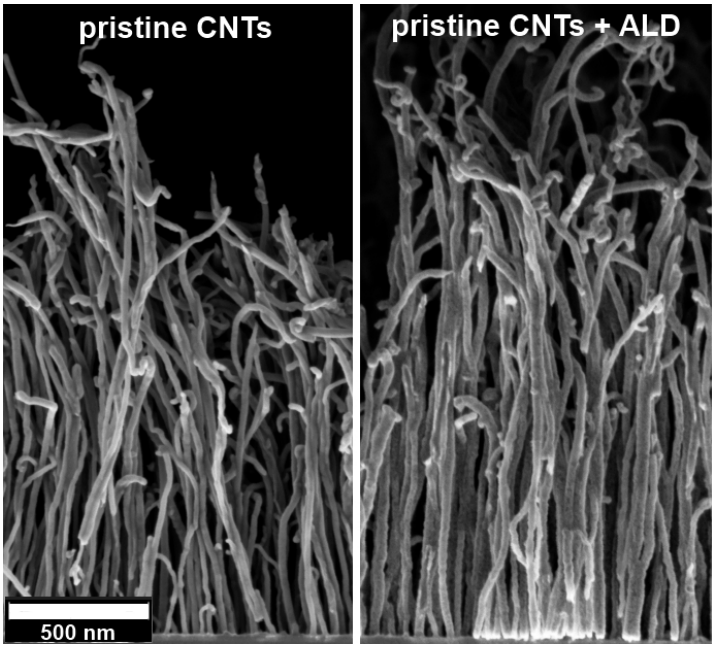

Figure 5.3: SEM images of pristine MWCNTs and pristine MWCNTs after 400 cycles Cu_xO ALD. The ALD causes a slight thickening of the CNTs. The scale bar of 500 nm applies to both images.

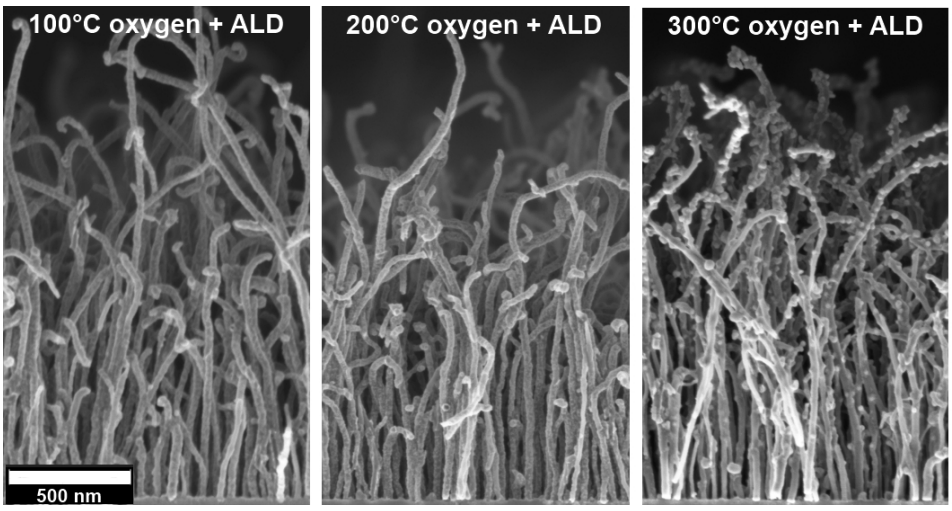

Figure 5.4: SEM images of MWCNTs after an oxidation at various temperatures with oxygen and 400 cycles Cu_xO ALD. NPs can be seen at the sample that was pretreated at 300°C. If the oxidation temperature is lower than 300°C, then the NPs are probably smaller and can only be resolved in the TEM images, analogous to the samples which were pretreated with wet oxygen. The scale bar of 500 nm applies to all images.

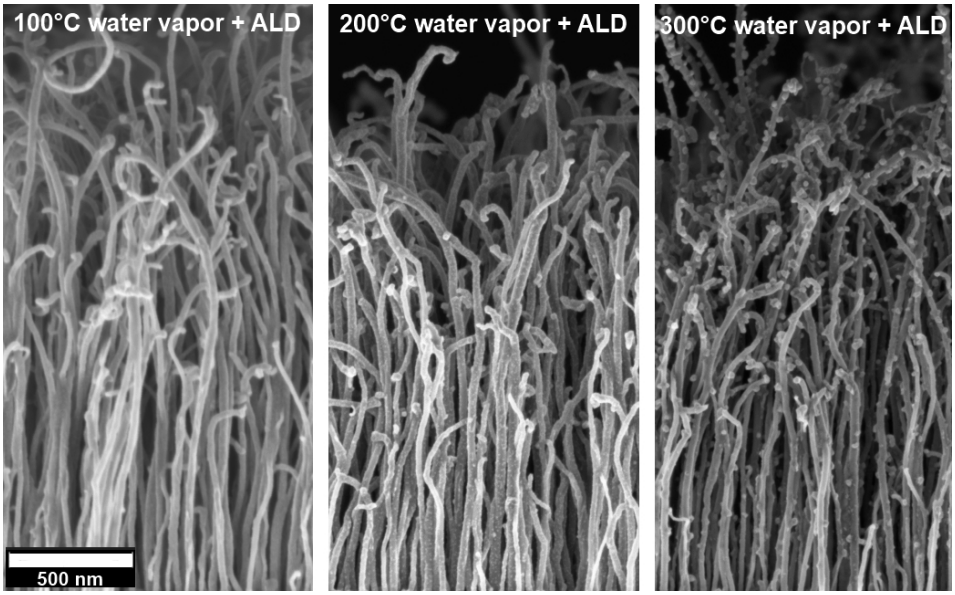

Figure 5.5: SEM images of MWCNTs after an oxidation at various temperatures with water vapor and 400 cycles Cu_xO ALD. NPs can be seen at the sample that was pretreated at 300°C. If the oxidation temperature is lower than 300°C, then the NPs are probably smaller and can only be resolved in the TEM images, analogous to the samples which were pretreated with wet oxygen. The scale bar of 500 nm applies to all images.

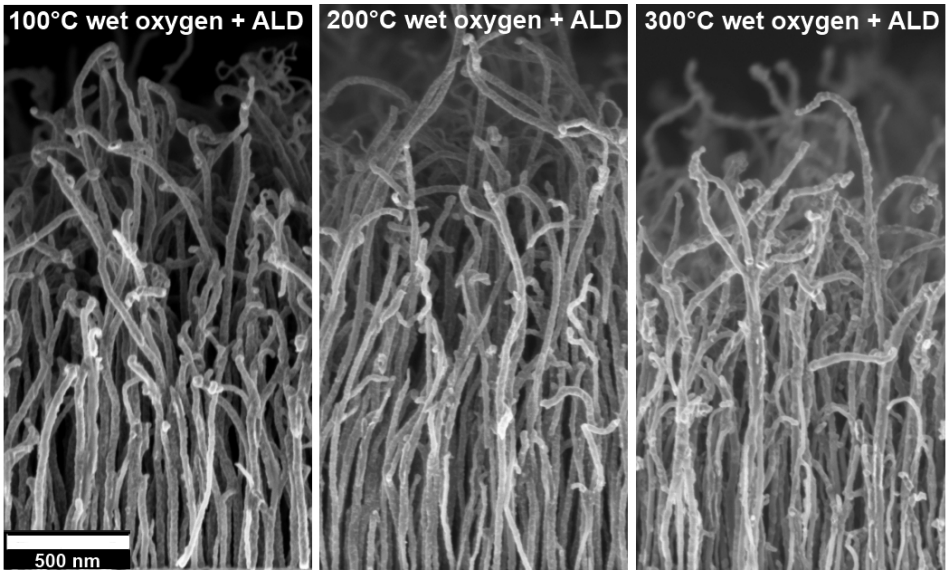

Figure 5.6: SEM images of MWCNTs after an oxidation at various temperatures with wet oxygen and 400 cycles Cu_xO ALD. NPs can be seen at the sample that was pretreated at 300°C. Compared to the other pretreatments at 300°C, those NPs are less sharply separated from the CNT. This can possibly be attributed to the partial destruction of the CNT sidewall, see text. If the oxidation temperature is lower than 300°C, then the NPs are smaller and can only be resolved in the TEM images, see Fig. 5.1 (a, b). The scale bar of 500 nm applies to all images.

The density of the NPs is higher at the top end of CNTs that stick out of the via. This can possibly be attributed to a higher defect density at the top edge of the CNTs and a higher amount of oxidation agent that gets in contact with the CNT surface outside of the vias.

The missing of NPs on the sample which was not pretreated before the ALD can possibly be explained with the stabilization of physisorbed reactive groups on the sidewalls of the CNTs [69]. These surface groups are physisorbed by van der Waals forces on the surface of the CNTs, independently of defect sites. Therefore, preferred nucleations site are missing. In contrast, the formation of NPs occurs probably only at defect sites of the CNTs, due to their higher reactivity [97]. A possible reason why NPs growth occurs on all samples except the unpretreated sample, is that the adsorption of new molecules from the oxidation agent occurs only at defect sites during the pretreatment , because there the binding energy is probably higher as in faultless areas of the carbon lattice.

Furthermore, the formation of NPs corresponds to the investigation of metal-tube interaction by Zhang et al. [16]. These experiments have shown that metals with a low number of d-electrons like Ti exhibit a high binding energy towards the CNT. In contrary, metals with fully occupied d-orbitals like Cu only show a low binding energy. This causes the formation of particles instead of a closed layer on the CNT surface.

The formation of bigger NPs at the 300°C O_2 and the 300°C H_2O sample can eventually be attributed to the attack of already existing defects by the oxidation with water or oxygen at elevated temperatures. It is known that aggressive oxidations can burn holes into the sidewalls [98]. It is expected that this happens at original defect sites due to their higher reactivity. The edges of those holes are eventually a preferred nucleation site for the precursor. Maybe the edges of these holes coalesce during the ALD. Possibly thereby the NPs are formed, which are visible in the SEM.

The NPs at the sample which was oxidized with wet oxygen at 300°C are not as sharply separated from the CNT like for the CNTs pretreated at 300°C with oxygen or water vapor, see Fig. 5.8 (a)-(c). In contrast, the sample which was oxidized with wet oxygen at 300°C indicates a rather layer-like growth mode. Eventually this can be attributed to the partial destruction of the sidewalls due to the oxidation with wet oxygen at 300°C, because it is known that on amorphous carbon layer-like growth occurs [99]. This becomes especially clear at the very reactive tips of the CNTs [100], see Fig. 5.7. It seems like a Cu_xO layer

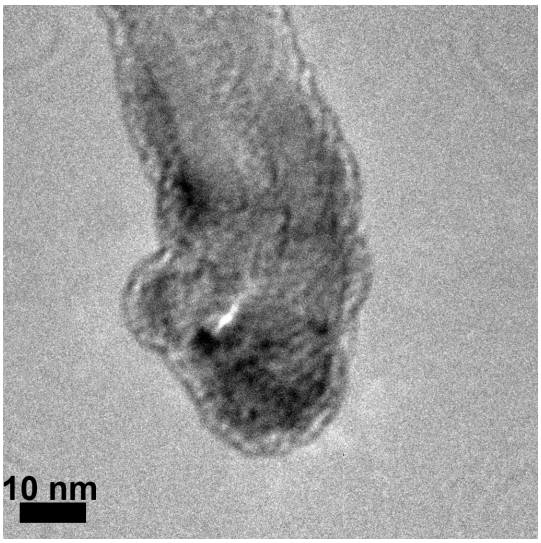

Figure 5.7: TEM image, which shows the tip of a CNT which was pretreated at 300°C with wet oxygen. This tip contains probably a piece of the Ni catalyst (dark circle). Furthermore, the tip area seems to be coated with a Cu_xO layer.

is formed around the hole tip of the CNT. However, eventually the layer which is visible in the TEM image shows only defects which have already been existing before the oxidation and the ALD. The possible destruction of the sidewalls probably occurs only with wet oxygen, since it is a more aggressive oxidation agent than oxygen or water vapor [101]. If the temperature of the wet oxygen pretreatment is below 300°C, the oxidation is not aggressive enough to attack the CNT sidewalls. In this case no amorphous carbon is formed and therefore again well-defined NPs are deposited, see Fig. 5.1 (a) and (b).

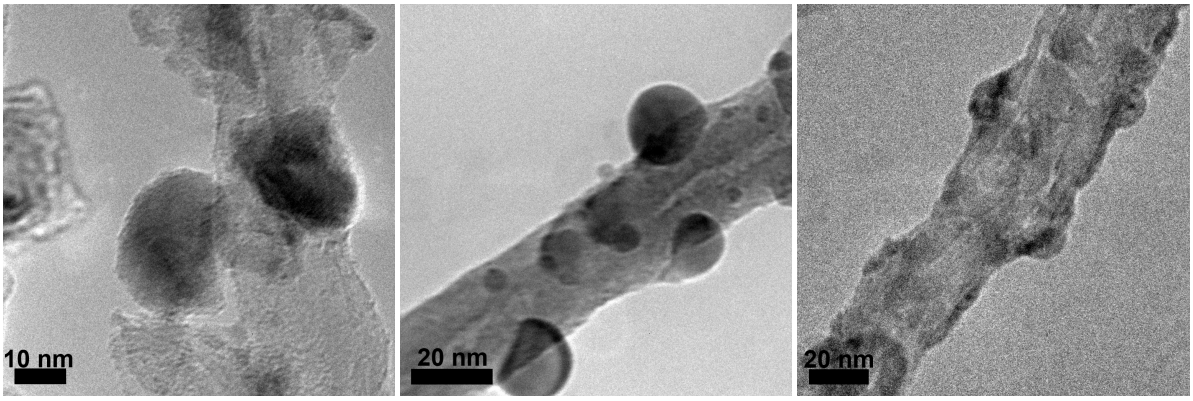

(a) 300°C H_2O (b) 300°C O_2 (c) 300°C H_2O+O_2

Figure 5.8: TEM images of differently pretreated CNTs after Cu_xO ALD. The samples that were oxidized at 300°C with water vapor or oxygen before ALD show relatively round NPs. In contrast, the NPs are rather flattened on the surface of CNTs which were oxidized with wet oxygen at 300°C , see subfigure (c).

The diffraction patterns of the samples which were pretreated at 300°C with oxygen or water vapor indicate the formation of crystalline Cu_xO NPs at the surface of the CNTs. That these NPs are crystalline is indicated by bright spots in the diffraction images, see Fig. 5.9 (a) and (b). These bright spots arise due to the preferred orientation of the Cu_xO crystals. In contrast amorphous Cu_xO would appear in the diffraction image as gray ring without any bright spots. Such an amorphous behavior is visible in the diffraction images of the samples which were pretreated with wet oxygen and the sample which was not oxidized before the ALD, see Fig. 5.9 (c)-(f). Eventually Cu_xO on the samples which were pretreated at 300°C with oxygen or water vapor are crystalline, because they are bigger compared to the NPs of the other samples, see SEM overview Fig. 5.2. For smaller NPs an amorphous state is eventually energetically preferred.

The diffraction reflexes of Cu, CuO and Cu_2O as well as the reflexes of graphite were applied to the acquired diffraction images of the samples which were oxidized with wet oxygen and water vapor at 300 °C. This has shown that the first bright circle is caused by the CNTs[1]. The comparison of Cu, CuO and Cu_2O has shown the best agreement of the expected reflexes and the acquired diffraction images for CuO. Therefore only the expected reflexes of CuO are illustrated in Fig. 5.9 (a) and (c). The

[1] The bright area in the center of the diffraction image is caused by electrons of the probe which has not interact with the sample.

agreement of CuO with the diffraction image indicates that during the ALD mainly CuO is deposited. This is supported by the results of the Raman spectroscopy, see *chapter 5.3*

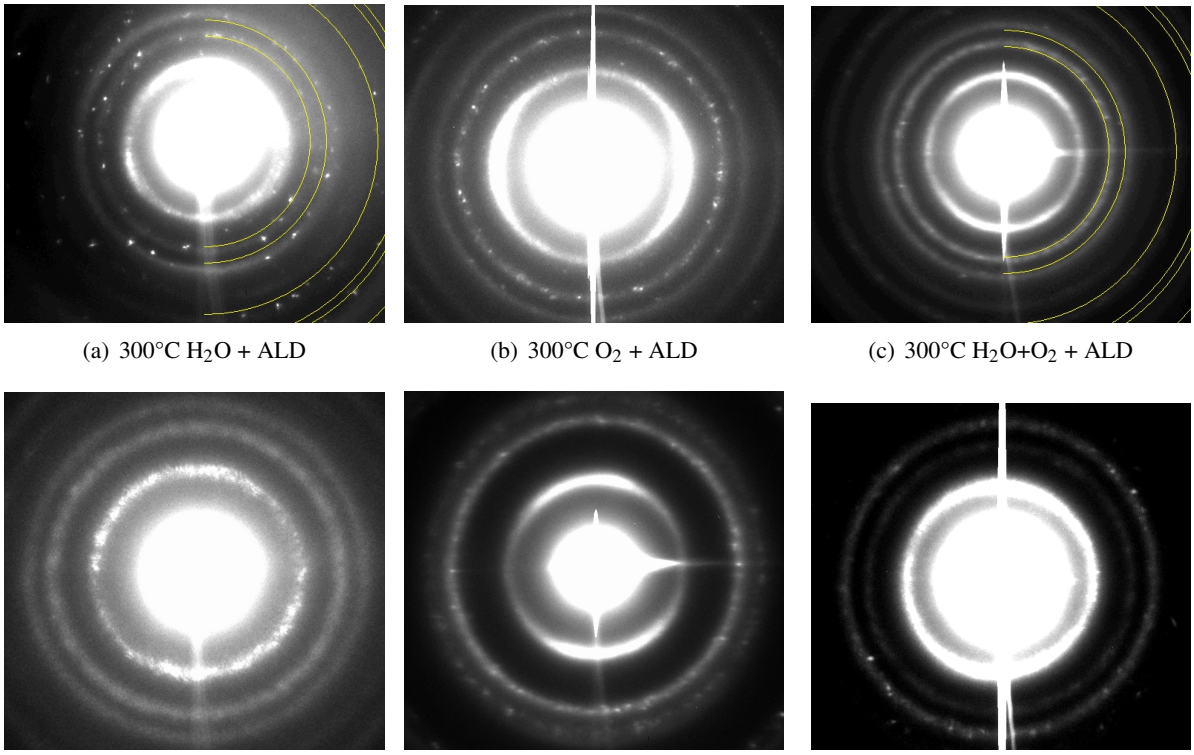

(a) 300°C H_2O + ALD (b) 300°C O_2 + ALD (c) 300°C H_2O+O_2 + ALD

(d) unpretreated CNTs + ALD (e) 100°C H_2O+O_2 (f) 200°C H_2O+O_2

Figure 5.9: Diffraction images of pretreated as well as unpretreated CNTs after Cu_xO ALD. The diffraction reflexes of CuO are marked in (a) and (c). If the sample is oxidized with oxygen or water vapor at 300°C many bright spots in the diffraction indicate the formation of cristalline NPs on the CNTs, see Fig. 5.8 (a,b). In contrast the diffraction image of the CNTs that were pretreated with wet oxygen at 300°C shows no bright spots. This is a hint that at these samples amorphous Cu_xO is deposited. If the CNTs are pretreated below 300°C with wet oxygen or remain unpretreated before the ALD, then only amorphous Cu_xO is deposited which is indicated by the missing of bright spots in the diffraction images.

5.2 Energy Dispersive X-ray Spectroscopy

As already mentioned in *chapter 4*, the EDX spectra were normalized to the C-peak to exclude the influence of different CNT densities of the samples. Since the copper oxide coating of the CNTs shields the C signal of the CNTs, the C value decreases with increasing copper oxide coverage. As a result the Cu/C ratio which is displayed in Fig. 5.10 increases not linear with the Cu_xO coating but quicker.

Fig. 5.11 exemplifies the EDX spectra of the samples which were oxidized with water vapor before the Cu_xO ALD and the CNT sample which was not oxidized before the ALD. It becomes apparent that the unpretreated sample has a Cu content that is approx. twice as high as the Cu content of the samples

that were oxidized before the ALD process. This can eventually be traced back to the desorption of functional groups from the surface of the CNTs during the pretreatment, which is not compensated by the adsorption of molecules from the oxidation agents. It is well known that ALD requires reactive surface groups. The possibly decreased number of surface groups due to desorption during the pretreatment would therefore cause a lower amount of deposited Cu_xO.

Thermogravimetric analysis (TGA) has shown that the moisture that accumulates on the CNTs during storage in air desorbs at temperatures below 100°C [102, 103]. Further experiments have shown that hydroxyl groups start desorbing from the CNTs around 150°C [104]. This desorption occurring during the pretreatment decreases the number of surface groups that are possibly reactive towards the precursor. Therefore, it is expected that less Cu_xO is deposited as already mention above.

The Cu/C ratios of the CNTs pretreated with oxygen drops out of this observation, see Fig. 5.10. A possible explanation is that the applied precursor need reactive oxygen surface groups. These groups are eventually introduced to the defect sites of the CNTs during the 30 min lasting pretreatment. Maybe this is enabled by the replacement of already existing reactive groups, which occupy the defect sites, by new oxygen groups from the oxidation agent due to the interplay of desorption and adsorption during the oxidation. The oxygen of the wet oxygen mixture is probably also the reason for the higher Cu_xO content of the wet oxygen samples compared to water vapor pretreated samples. This conclusion is supported by the results of the ellipsometry measurements of the SiO_2 monitoring samples, see *chapter 5.4*.

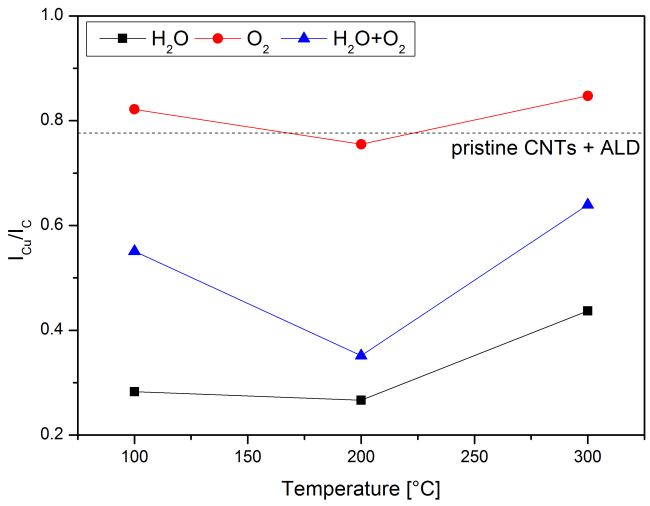

Figure 5.10: Cu/C ratios of all CNT samples that were prepared. The Cu content of water vapor and wet oxygen pretreated CNT is smaller than the Cu content of the samples that were oxidized with oxygen. This can be interpreted as a hint that the used copper precursor requires oxygen surface groups. The dotted line marks the Cu/C ratio of the sample which was not pretreated before the ALD.

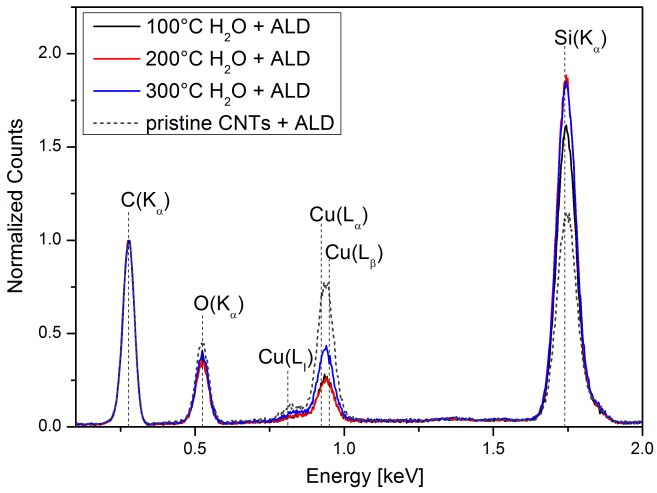

Figure 5.11: EDX spectra of pristine CNTs after Cu_xO ALD and the CNT samples which were oxidized with H_2O at various temperatures and coated with 400 cycles ALD. The spectra are normalized to the carbon peak. The Cu content of the pretreated samples is smaller than the copper content of the sample that was not oxidized before ALD. This suggests the desorption of functional groups from the CNTs during the pretreatment. The different peaks are discussed in the text.

5.3 Raman Spectroscopy

Raman spectroscopy was carried out on all CNTs samples to evaluate the damage introduced to the CNTs during the oxidation and the ALD process. Besides this, a sample with pristine CNTs was examined as well as a SiO_2 substrate and a SiO_2 substrate with a Cu_xO ALD film on top. The comparison of the SiO_2 samples with and without Cu_xO layer has shown that no Cu_xO is detectable with the used experimental set up (UV laser, $\lambda = 325$ nm) due to the small film thickness.

In contrast, on the CNTs additional peaks are detectable at 177, 290 and 625 cm^{-1} after the Cu_xO ALD, see Fig. 5.12. A reason for it is possibly the distribution of the Cu_xO NPs over the complete height of the CNTs (approx. 2 μm) and therefore a higher amount of Cu_xO with which the light ray can interact compared to the plane SiO_2 sample. The peaks at 177 and 625 cm^{-1} align not well with the values for CuO and Cu_2O found in the literature [105, 106]. Eventually these Raman peaks are dispersive and shift with the used wavelength. However, whether these peaks are dispersive is not reported in the literature. With the measurements which were performed with the green laser ($\lambda = 514$ nm) this prediction cannot be checked, because with the green laser the Raman shift was only measured around the D and G-peak, but not in the area of the Cu_xO peaks. The literature values for CuO align well with the peak at 290 cm^{-1}. Eventually this good alignment arises because during the ALD process mainly CuO is deposited on the CNTs. This conclusion is supported by the diffraction images in *chapter 5.1*, because the diffraction rings align also best with the data for CuO.

Fig. 5.13 shows a typical Raman spectrum of MWCNTs. In the range from 150 to 650 cm^{-1} a plateau can be seen. This feature arises from the overlap of radial breathing mode peaks (RBM), a silicon peak at 320 cm^{-1} [96] and the above mentioned Cu_xO peaks. The RBM peaks can be used to determine the diameter of a SWCNT, but due to the different diameters that appear in MWCNT samples those peaks smear to the measured plateau. The two main features of this spectrum are the D-peak (1400 cm^{-1}) and the G-peak (1580 cm^{-1}). For the determination of the defect density of the CNTs via the I_D/I_G ratio it is important that at the D and the G-peak no Cu_xO peaks appear, see inset Fig. 5.13. At the end of the measurement range, a peak can be detected which arises from the overlap of the overtone of the D-band (mostly labeled with G') and the overtone of an LO mode.

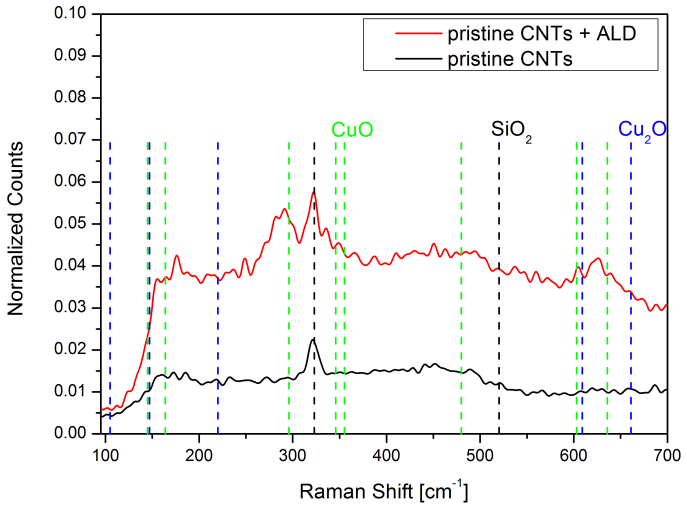

Figure 5.12: Raman spectra of pristine CNTs and pristine CNTs after 400 ALD cycles. The various colored lines mark the position of the Raman peaks of CuO [106] and Cu_2O [105] as well as the peaks of SiO_2, which rely on own measurements. The good accordance of the additional peak at 290 cm^{-1} indicates that during the ALD mainly CuO is deposited. For the measurement a UV laser ($\lambda = 325$ nm) was used.

For the determination of the defect density a green laser ($\lambda = 514$ nm) was applied to gain a higher accuracy, because with the green laser the D-peak rises clearly, compared to the G-band. Fig. 5.14 exemplifies the D and G-band of the CNTs which were pretreated with water vapor as well as the data of pristine CNTs and CNTs which were not oxidized before the ALD.

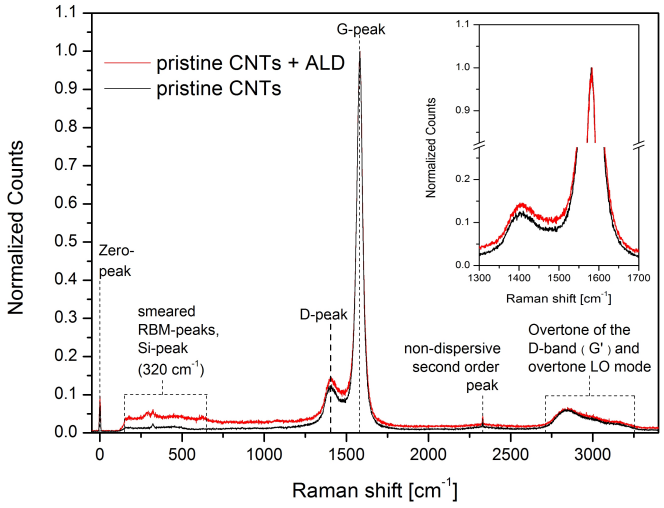

Figure 5.13: Raman spectra of pristine CNTs and CNTs which were not oxidized before ALD. On the scale which is used in this image no peaks are visible that arise due to the Cu_xO, for it see Fig. 5.12. At the D and G-band no additional peaks are visible after the ALD, see inset. The different peaks are described in the text. For the measurement a UV laser ($\lambda = 325$ nm) was used.

Fig. 5.15 shows the I_D/I_G ratio of the CNT samples which is proportional to the defect density. The comparison of the measured I_D/I_G ratio differences with further measurements carried out in our institution or published in papers makes clear that the variations in the I_D/I_G ratio of the CNTs samples examined within this thesis are small[2] [35]. The difference between the biggest and the smallest value of the I_D/I_G ratio is 0.1. Analysis of the influence of the temperature during the CNT growth of the used CNT samples has shown a variation of the I_D/I_G ratio by 0.7 [11, p. 76-79]. Therefore the measured differences can probably be traced back to variations of the I_D/I_G ratio caused by different positions of the samples on the wafer and measurement errors. For this reason the Raman measurements suggest that the CNTs are not or only slightly attacked during the pretreatment. This is congruent with the experiments of Bu et al. [35].

The offset between the samples pretreated with water vapor (as well as the pristine and unpretreated sample) and the samples which were oxidized with oxygen or wet oxygen is eventually caused by slightly different measurement conditions, because the samples were examined on various days.

In *chaper 5.1* a partial destruction of the CNT sidewalls was indicated by a rather layer-like Cu_xO growth at the sample which was pretreated with wet oxygen at 300°C. However, the expected destruction of the sidewalls is not reflected by the Raman measurements. Eventually the part of the CNTs which is attacked during the pretreatment is to small too be detected by Raman spectroscopy.

[2]The comparison of Raman spectra performed with different measurement set ups is always a little bit doubtful because the intensity of the different peaks and therefore the I_D/I_G ratio strongly depends on the used light source. For example, the difference in the I_D/I_G ratio of various samples disappeared in the noise when the UV laser was used for excitation.

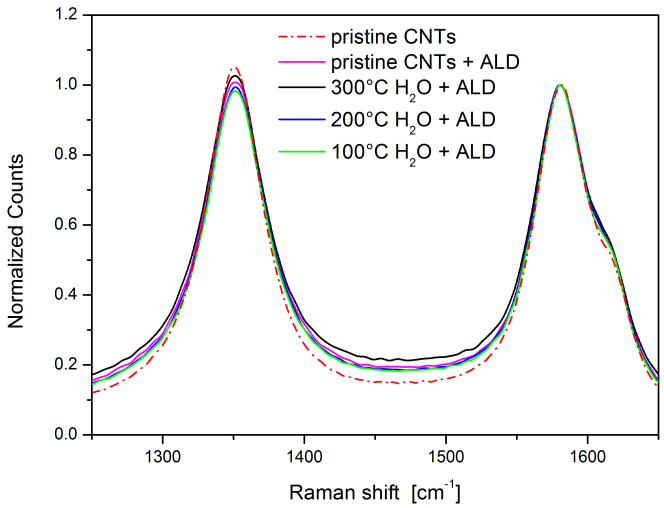

Figure 5.14: Raman spectra of pristine CNTs, pristine CNTs after ALD and CNTs which were oxidized with H_2O at various temperatures and treated with 400 cycles ALD. The change in the height of the D-peak is small. For this measurement a green laser ($\lambda = 514$ nm) was used.

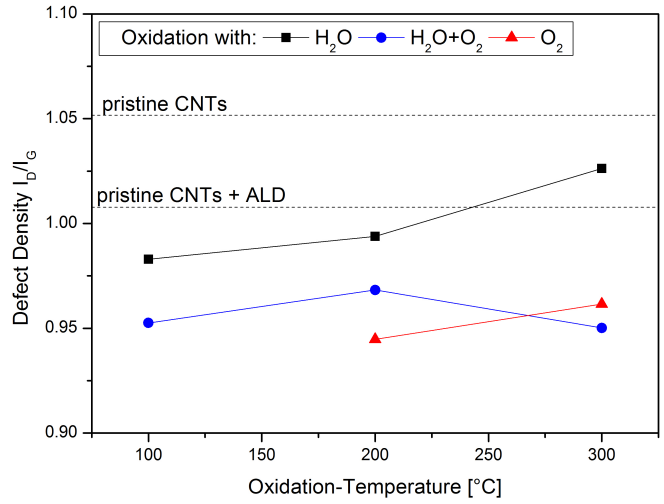

Figure 5.15: I_G/I_D ratio, which is proportional to the defect density of the CNTs. Compared to other measurements the differences between the various samples are small and can probably traced backed to variability of the crystallinity of the samples depending on the position of the CNTs on the wafer, see text. The dotted lines mark the I_G/I_D ratios of pristine CNTs before and after the ALD. For this measurement a green laser ($\lambda = 514$ nm) was used.

5.4 Spectroscopic Ellipsometry

Additionally to the CNT samples always also a SiO_2 substrate was placed within the ALD reactor during the pretreatment and the subsequent ALD process to monitor the ALD process. For the evaluation of the ALD process the SiO_2 samples were characterized by SE after the ALD. With these SE data the Cu_xO film thicknesses was calculated, see Fig. 5.16. However, the ellipsometry software SpectraRay 2 requires the properties of the substrate on which the Cu_xO layer is deposited for the calculation of the Cu_xO film thickness. Therefore a SiO_2 wafer (20 nm dry SiO_2 on Si) was characterized via SE. The film thickness as well as the optical properties were calculated via SpectraRay 2. Afterwards, this wafer was split into the SiO_2 samples which were later used for the monitoring of the ALD process.

Furthermore, three SiO_2 substrates were oxidized with wet oxygen and afterwards characterized via SE to determine how strong the influence of the pretreatment onto the SiO_2 layer and the subsequent fitting of the spectroscopic ellipsometry data is. The analysis of these measurements have been applied to the film thickness calculations of the samples which were pretreated with wet oxygen. The results are plotted in Fig. 5.16. The change of the SiO_2 during the pretreatment causes a slight offset of the calculated film thicknesses. However, the shape of the curve is not changed. The offset is expected to be maximal if the sample is treated with wet oxygen because wet oxygen is expected to be the most aggressive oxidation agent [101].

Eventually the SE results are influenced by a changing film morphology of the Cu_xO due to the pretreatment. This must still be checked by SEM images of the coated SiO_2 samples.

It is observable that the film thickness and therefore the amount of deposited Cu_xO depends on the oxidation agent and the oxidation temperature. Independently of the oxidation agent the Cu_xO film thickness decreases when the oxidation temperature is increased from 100°C to 200°C, see Fig. 5.16. It is well known that ALD depends strongly on the presence of reactive surface groups. Which surface groups are required depends on the applied precursor. That the film thickness decreases between 100 and 200°C can possibly be explained with the desorption of required surface groups during the pretreatment. The desorption of reactive surface groups is possibly also the reason why the film thickness of the samples which were pretreated with oxygen, water vapor or wet oxygen at 100 and 200°C is smaller than the unpretreated sample, see Fig. 5.16. Possible surface groups that desorbs during the pretreatment are physisorbed moisture or other weakly bonded organic contaminations which accumulate on the sample surface during the storage in air.

However, besides desorption always also adsorption occurs. Nevertheless, the results indicate that the desorption rate is bigger then the adsorption rate, because although the samples are surrounded by the oxidation agent it seems like the amount of surface groups decreases because the film thickness decreases with the pretreatment. Eventually, the interplay of desorption and adsorption causes the replacement of already existing surface groups by new surface groups from the oxidation agent during the pretreatment. This would for example mean that for the oxidation with oxygen the SiO_2 surface is possibly predominantly occupied with oxygen groups. Because the film thickness is the biggest for the samples which were pretreated with oxygen this chain of thought would mean that the applied precursor requires oxygen groups. This consideration that the ALD process works best with reactive

oxygen surface groups is supported by the results of the EDX measurements of the CNTs coated with Cu_xO, see *chapter 5.2*. It is also known that on dry SiO_2 a higher GPC occurs than on wet silicon dioxide [12, p. 98-108]. Maybe this can also be attributed to a higher amount of oxygen groups on the dry silicon dioxide which was grown by oxidation of silicon with oxygen (dry oxide) instead of water (wet oxide).

In contrast, if the temperature is further increased to 300°C, the film thickness increases obviously. It is well known that the surface of SiO_2 is occupied by OH groups. Possibly at temperatures above 200°C further molecules bind to these groups by a hydrogen bond. These groups may serve as starting points for the ALD. Eventually these groups increase the density of areas where Cu_xO deposition occurs during the first ALD cycles. Maybe this increased nucleation site density causes the faster formation of a closed ALD layer which enables a higher GPC in the subsequent ALD cycles. This behavior, that the GPC increases clearly after the formation of a closed starting layer is already known from other ALD processes [107]. This change in GPC is attributed to the initial growth of islands and their subsequent coalescence. Maybe this state is faster obtained at the samples which were pretreated at 300°C due to the higher number of nucleation sites. Therefore at these samples a higher number of ALD cycles is carried out with a high GPC instead of the cycles at the beginning of the ALD process with low GPC. This could cause the higher values for the Cu_xO film thickness at 300°C oxidation temperature.

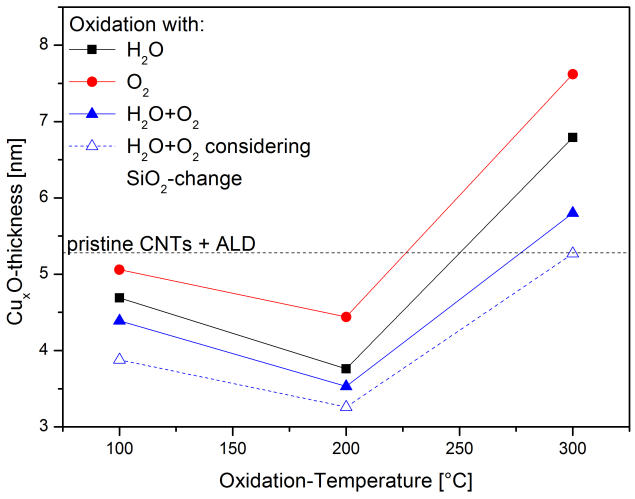

Figure 5.16: Cu_xO film thickness after 400 ALD cycles at 135°C on SiO_2 substrates. If the various oxidation agents are compared it is observable that by pretreatment with O_2 the biggest film thickness can be achieved, independently of the pretreatment temperature. Eventually this can be explained with the need for reactive oxygen groups of the used precursor. The thickness was calculated from the SE data.

6 Summary and Outlook

The integration of CNTs in ULSI metallization systems or in sensors devices requires the functionalization of the MWCNTs. One example for the functionalized CNTs is the deposition of metals or metal oxides on the surface of the CNTs. Due to the high aspect ratio of CNTs an appropriate deposition technique has to be applied which is able to coat such structures uniformly. Therefore this thesis examined the influence of different oxidation agents (oxygen, water vapor and wet oxygen) and different oxidation temperatures on a subsequent Cu_xO ALD on MWCNTs, see Tab. 6.1.

The analyses of the various samples have shown that by variation of the pretreatment parameters the shape of the deposited copper oxide can be controlled. On CNTs which were not oxidized before the ALD, the copper oxide was deposited on the CNTs without any recognizable structure. In contrast, small NPs, which were only resolvable in the TEM, have been formed at the MWCNTs which were pretreated with wet oxygen at temperatures up to 200°C. Although no TEM images were acquired of the samples which were oxidized at 100 and 200°C with oxygen or water vapor, it is expected that also on these MWCNTs small NPs have been deposited. However, of these two oxidation agents only TEM images have been acquired of the CNTs which were oxidized at 300°C . If the temperature during the pretreatment is increased to 300°C and water vapor or oxygen is applied as oxidation agent, bigger NPs with a diameter of approx. 10 nm can be formed on the CNTs. These NPs are probably generated on defect sites of the CNTs due to their higher reactivity. The diffraction images indicate that these NPs are crystalline.

A partially rather layer-like Cu_xO growth can be achieved if the MWCNTs are pretreated with wet oxygen at 300°C. The article by Egelhoff et al. suggests that this behavior can be traced back to a partial destruction of the CNT sidewalls [99]. Probably the oxidation attacks only the areas around already existing defect sites, because the areas were Cu_xO has been deposited on the CNTs have some kind of center with a NP which is partially embedded into the layer like grown copper oxide around. Eventually, this center is located at the primary defect. The diffraction image of the sample which was pretreated with wet oxygen at 300°C indicates that the deposited Cu_xO is amorphous.

The damage that is introduced to the CNTs during the pretreatment and the ALD is low, because the variations in I_D/I_G ratio of the different pretreated samples are small, compared to other references [11, p. 76-79]. Eventually, these differences are caused by variations during the CNT growth and by different position of the samples on the wafer.

EDX measurements and SE measurements indicate that the used Cu_xO ALD process requires reactive oxygen surface groups, see Tab. 6.1. Future investigations of the ALD process via in-situ XPS should enhance the knowledge of the used Cu(I) β-diketonate ALD process and its surface chemistry.

For the potential application of the ALD treated CNTs in metallization structures the reduction of the Cu_xO to metallic copper is necessary. Therefore the transition of Cu_xO to metallic copper by various approaches should be examined [12, p. 121-135]. To verify the influence of the Cu NPs onto the electrical properties of the MWCNTs, electrical measurements are required. However, it is still a challenge to contact the MWCNTs which are embedded in vias. Nevertheless, those electrical measurements are needed to compare the influence of the Cu NPs onto the conductance and the contact resistance of the CNTs with other already examined metals like Ti and Pt [14, 108].

Table 6.1: Overview of the results of various pretreatments onto a subsequent Cu_xO ALD. The ALD was performed for 400 cycles at a pressure of 1.33 mbar and a temperature of 135°C. The used precursor was $[(^nBu_3P)_2Cu(acac)]$. The various oxidations are grouped by the temperature, to make clear that the I_{Cu}/I_C ratio of the CNTs and the film thickness on SiO_2 is always greatest when the sample was pretreated with oxygen.

oxidation agent	**T [°C]**	**SEM NPs visible**	**TEM NPs visible**	**structure of Cu_xO**	**I_{Cu}/I_C EDX[3]**	**I_D/I_G Raman shift[4]**	**film thickness on SiO_2[5] [nm]**
O_2		no	-[1]	-[1]	0.82	-	5.1
H_2O	**100°C**	no	-[1]	-[1]	0.28	0.98	4.7
H_2O+O_2		no	yes	amorphous	0.55	0.95	4.4
O_2		no	-[1]	-[1]	0.76	0.95	4.4
H_2O	**200°C**	no	-[1]	-[1]	0.27	1.00	3.8
H_2O+O_2		no	yes	amorphous	0.35	0.97	3.5
O_2		yes	yes	crystals	0.85	0.96	7.6
H_2O	**300°C**	yes	yes	crystals	0.43	1.03	6.8
H_2O+O_2		yes	yes + layer[2]	amorphous	0.64	0.95	5.8

[1] This measurement was not performed. Nevertheless, it is expected that the results would be analog to the sample which was oxidized with wet oxygen at the same temperature.
[2] The NPs are embedded into a area of rather layer-like growth.
[3] The I_{Cu}/I_C value for the sample which was not oxidized before ALD is 0.78.
[4] The I_D/I_G ratio of pristine CNTs is 1.05 and the value of the sample which was not oxidized before ALD is 1.01.
[5] The film thickness of the sample which was not oxidized before ALD was 5.3 nm.

Bibliography

[1] L. Radushkevich and V. Lukyanovich, "O strukture ugleroda, obrazujucegosja pri termiceskom razlozenii okisi ugleroda na zeleznom kontakte", *Zurn Fisic Chim* **26**, 88–95, 1952.

[2] M. Monthioux and V. L. Kuznetsov, "Who should be given the credit for the discovery of carbon nanotubes?", *Carbon* **44**(9), 1621 – 1623, 2006.

[3] S. Iijima, "Helical microtubules of graphitic carbon", *Nature* **354**(6348), 56–58, 1991. cited By (since 1996) 17661.

[4] M. Dresselhaus, G. Dresselhaus, and P. Avouris, *Carbon nanotubes: synthesis, structure, properties, and applications*, vol. 80 of *Topics in applied physics*, ch. Applications of Carbon Nanotubes, 391–425. Springer, 1 ed., 2001.

[5] M. Daenen, R. de Fouw, B. Hamers, P. Janssen, K. Schouteden, and M. Veld, "The Wondrous World of Carbon Nanotubes: a review of current carbon nanotube technologies. 13/10/2011 (`http://students.chem.tue.nl/ifp03/Wondrous%20World%20of%20Carbon%20Nanotubes_Final.pdf`)", 2003.

[6] Nanoscience Instruments, AFM Probes: Nanotube Tips. 13/10/2011 (`http://www.nanoscience.com/store/pc/viewCategories.asp?idCategory=9`).

[7] http://nanotechweb.org, "Nanotube bike enters Tour de France. 13/10/2011 (`http://nanotechweb.org/cws/article/tech/22597`)", 2005.

[8] M. S. Purewal, B. H. Hong, A. Ravi, B. Chandra, J. Hone, and P. Kim, "Scaling of Resistance and Electron Mean Free Path of Single-Walled Carbon Nanotubes", *Phys. Rev. Lett.* **98**, 186808, May 2007.

[9] S. Hunklinger, *Festkörperphysik*, ch. 8, 264–269. Oldenburg Verlag, 2009.

[10] R. Saito, G. Dresselhaus, and M. Dresselhaus, *Physical Properties of Carbon Nanotubes*, Imperial College Press, 1998.

[11] S. Hermann, *Growth of carbon nanotubes on different support/catalyst systems for advanced interconnects in integrated circuits*. PhD thesis, TU Chemnitz, 2011.

[12] T. Waechtler, *Thin Films of Copper Oxide and Copper grown by Atomic Layer Depostition for Applications in Metallization System of Microelectronic Devices*. PhD thesis, TU Chemnitz, 2009.

[13] SEMATECH, SIA, TSIA, KSIA, JEITA, and ESIA, eds., *ITRS - The International Technology Roadmap for Semiconductors*, 2009 Edition and 2010 Update (`http://www.itrs.net/reports.html`).

[14] Y. Kim, B. Li, X. An, M. Hahm, L. Chen, M. Washington, P. Ajayan, S. Nayak, A. Busnaina, S. Kar, and Y. Jung, "Highly aligned scalable platinum- decorated single-wall carbon nanotube arrays for nanoscale electrical interconnects", *ACS Nano* **3**(9), 2818–2826, 2009.

[15] J. Sommer, "Ab initio Berechnung des Elektronentransports in metallbeschichteten Kohlenstoffnanoröhrchen", bachelor thesis, Fraunhofer ENAS/ TU Chemnitz, 2011.

[16] Y. Zhang, N. W. Franklin, R. J. Chen, and H. Dai, "Metal coating on suspended carbon nanotubes and its implication to metal-tube interaction", *Chemical Physics Letters* **331**(1), 35–41, 2000.

[17] J. Yeow and Y. Wang, "A review of carbon nanotubes-based gas sensors", *Journal of Sensors* **Volume 2009**, 24 pages, 2009.

[18] Q. Zhao, M. Buongiorno Nardelli, W. Lu, and J. Bernholc, "Carbon Nanotube-Metal Cluster Composites: A New Road to Chemical Sensors?", *Nano Letters* **5**(5), 847–851, 2005.

[19] P. Samarasekara, N. T. R. N. Kumara, and N. U. S. Yapa, "Sputtered copper oxide (CuO) thin films for gas sensor devices", *Journal of Physics: Condensed Matter* **18**(8), 2417–2420, 2006.

[20] B. Lee, S.-Y. Park, H.-C. Kim, K. Cho, E. Vogel, M. Kim, R. Wallace, and J. Kim, "Conformal Al_2O_3 dielectric layer deposited by atomic layer deposition for graphene-based nanoelectronics", *Applied Physics Letters* **92**(20), 203102 –203102–3, 2008.

[21] R. L. Puurunen and W. Vandervorst, "Island growth as a growth mode in atomic layer deposition: A phenomenological model", *Journal of Applied Physics* **96**(12), 7686–7695, 2004.

[22] T. Suntola and J. Antson, "Method for producing compound thin films", Patent, US 4,058,430, 1977.

[23] M. Ritala and M. Leskelä, "Atomic Layer Deposition", in *Handbook of Thin Film Materials. Vol. 1 – Deposition and Processing of Thin Films*. H. S. Nalwa, ed., 103–159, Academic Press, 2002.

[24] A. C. Jones, H. C. Aspinall, P. R. Chalker, R. J. Potter, K. Kukli, A. Rahtu, M. Ritala, and M. Leskela, "Some recent developments in the MOCVD and ALD of high-k dielectric oxides", *J. Mater. Chem.* **14**, 3101–3112, 2004.

[25] H. Kim, H.-B.-R. Lee, and W.-J. Maeng, "Applications of atomic layer deposition to nanofabrication and emerging nanodevices", *Thin Solid Films* **517**(8), 2563–2580, 2009.

[26] T. Aaltonen, *Atomic Layer Deposition of Noble Metal Thin Films*. PhD thesis, University of Helsinki, 2005.

[27] L. Niinistö, J. Nieminen, M.Päiväsaari, J. Niinistö, M. Putkonen, and M. Nieminen, "Advanced electronic and optoelectronic materials by Atomic Layer Deposition: An overview with special emphasis on recent progress in processing of high-k dielectrics and other oxide materials", *physica status solidi (a)* **201**(7), 1443–1452, 2004.

[28] R. L. Puurunen, "Surface chemistry of atomic layer deposition: A case study for the trimethylaluminum/water process", *Journal of Applied Physics* **97**(12), 121301, 2005.

[29] R. L. and Puurunen, "Correlation between the growth-per-cycle and the surface hydroxyl group concentration in the atomic layer deposition of aluminum oxide from trimethylaluminum and water", *Applied Surface Science* **245**(1-4), 6 – 10, 2005.

[30] T. Waechtler, S. Oswald, N. Roth, A. Jakob, H. Lang, R. Ecke, S. Schulz, T. Gessner, A. Moskvinova, S. Schulze, and M. Hietschold, "Copper Oxide Films Grown by Atomic Layer Deposition from Bis(tri-n-butylphosphane)copper(I)acetylacetonate on Ta, TaN, Ru and SiO_2", *Journal of The Electrochemical Society* **156**(6), H453–H459, 2009.

[31] E. E. Wu, L., "Hydrogen plasma-enhanced atomic layer deposition of copper thin films", *Journal of Vacuum Science and Technology B: Microelectronics and Nanometer Structures* **25**(6), 2581–2585, 2007.

[32] A. Niskanen, A. Rahtu, T. Sajavaara, K. Arstila, M. Ritala, and M. Leskelä, "Radical-enhanced atomic layer deposition of metallic copper thin films", *Journal of the Electrochemical Society* **152**(1), G25–G28, 2005.

[33] T. Toerndahl, M. Ottosson, and J.-O. Carlsson, "Growth of copper metal by atomic layer deposition using copper(I)chloride, water and hydrogen as precursors", *Thin Solid Films* **458**, 129–136, 2004.

[34] M.-A. Nicolet, "Diffusion barriers in thin films", *Thin Solid Films* **52**(3), 415 – 443, 1978.

[35] I. Y. Bu, K. Hou, and D. Engstrom, "Industrial compatible re-growth of vertically aligned multiwall carbon nanotubes by ultrafast pure oxygen purification process", *Diamond and Related Materials* **20**(5-6), 746 – 751, 2011.

[36] R. Solanki and B. Pathangey, "Atomic Layer Deposition of Copper Seed Layers", *Electrochemical and Solid-State Letters* **3**(10), 479–480, 2000.

[37] S. Gandikota, S. Voss, R. Tao, A. Duboust, D. Cong, L.-Y. Chen, S. Ramaswami, and D. Carl, "Adhesion studies of CVD copper metallization", *Microelectronic Engineering* **50**(1-4), 547 – 553, 2000.

[38] P. Martensson and J.-O. Carlsson, "Atomic Layer Epitaxy of Copper", *Journal of The Electrochemical Society* **145**(8), 2926–2931, 1998.

[39] B. S. Lim, A. Rahtu, and R. G. Gordon, "Atomic layer deposition of transition metals", *Nature Materials 2* **2**, 749–754, 2003.

[40] B. S. Lim, A. Rahtu, J.-S. Park, and R. G. Gordon, "Synthesis and Characterization of Volatile, Thermally Stable, Reactive Transition Metal Amidinates", *Inorganic Chemistry* **42**(24), 7951–7958, 2003.

[41] C. A. Rottmair, *Einfluss der thermischen Prozessführung auf die Eigenschaften von Graphitformteilen, hergestellt durch Pulverspritzguss von Mesophasen-Kohlenstoff*. PhD thesis, Universitïät Erlangen-Nürnberg, 2007.

[42] R. V. Seidel, *Carbon Nanotube Devices*. PhD thesis, TU Dresden, 2004.

[43] M. D. Ventra, S. Evoy, and J. R. Helfin, *Introduction to Nanoscale Science and Technology*, vol. 1, Springer, 2004.

[44] T. Belin and F. Epron, "Characterization methods of carbon nanotubes: a review", *Materials Science and Engineering B* **119**, 105–108, 2005.

[45] P. Lambin, "Electronic structure of carbon nanotubes", *Comptes Rendus Physique* **4**(9), 1009–1019, 2003.

[46] N. Hamada, S.-i. Sawada, and A. Oshiyama, "New one-dimensional conductors: Graphitic microtubules", *Phys. Rev. Lett.* **68**, 1579–1581, Mar 1992.

[47] T. W. Ebbesen and P. M. Ajayan, "Large-scale synthesis of carbon nanotubes", *Nature* **358**, 220–222, 1992.

[48] T. Guo, P. Nikolaev, A. Thess, D. Colbert, and R. Smalley, "Catalytic growth of single-walled manotubes by laser vaporization", *Chemical Physics Letters* **243**(1-2), 49 – 54, 1995.

[49] P. Ajayan, J. Lambert, P. Bernier, L. Barbedette, C. Colliex, and J. Planeix, "Growth morphologies during cobalt-catalyzed single-shell carbon nanotube synthesis", *Chemical Physics Letters* **215**(5), 509 – 517, 1993.

[50] D. Zhou, S. Seraphin, and S. Wang, "Single walled carbon nanotubes growing radially from YC2 particles", *Applied Physics Letters* **65**(12), 1593–1595, 1994.

[51] S. Seraphin, "Single-Walled Tubes and Encapsulation of Nanocrystals into Carbon Clusters", *Journal of The Electrochemical Society* **142**(1), 290–297, 1995.

[52] Z. F. Ren, Z. P. Huang, D. Z. Wang, J. G. Wen, J. W. Xu, J. H. Wang, L. E. Calvet, J. Chen, J. F. Klemic, and M. A. Reed, "Growth of a single freestanding multiwall carbon nanotube on each nanonickel dot", *Applied Physics Letters* **75**(8), 1086–1088, 1999.

[53] N. Inami, M. A. Mohamed, E. Shikoh, and A. Fujiwara, "Synthesis-condition dependence of carbon nanotube growth by alcohol catalytic chemical vapor deposition method", *Science and Technology of Advanced Materials* **8**(4), 292, 2007.

[54] J. Kong, A. M. Cassell, and H. Dai, "Chemical vapor deposition of methane for single-walled carbon nanotubes", *Chemical Physics Letters* **292**(4-6), 567 – 574, 1998.

[55] M. Ruemmeli, A. Bachmatiuk, F. Boerrnert, F. Schaeffel, I. Ibrahim, K. Cendrowski, G. Simha-Martynkova, D. Placha, E. Borowiak-Palen, G. Cuniberti, and B. Buechner, "Synthesis of carbon nanotubes with and without catalyst particles", *Nanoscale Research Letters* **6**, 1–9, 2011.

[56] P.-X. Hou, C. Liu, and H.-M. Cheng, "Purification of carbon nanotubes", *Carbon* **46**(15), 2003 – 2025, 2008.

[57] S. Banerjee, T. Hemraj-Benny, and S. Wong, "Covalent Surface Chemistry of Single-Walled Carbon Nanotubes", *Advanced Materials* **17**(1), 17–29, 2005.

[58] D. B. Mawhinney, V. Naumenko, A. Kuznetsova, J. T. Y. Jr., J. Liu, and R. Smalley, "Surface defect site density on single walled carbon nanotubes by titration", *Chemical Physics Letters* **324**(1-3), 213 – 216, 2000.

[59] A. Hirsch, "Functionalization of Single-Walled Carbon Nanotubes", *Angewandte Chemie International Edition* **41**(11), 1853–1859, 2002.

[60] R. J. Chen, Y. Zhang, D. Wang, and H. Dai, "Noncovalent Sidewall Functionalization of Single-Walled Carbon Nanotubes for Protein Immobilization", *Journal of the American Chemical Society* **123**(16), 3838–3839, 2001.

[61] M. J. O'Connell, S. M. Bachilo, C. B. Huffman, V. C. Moore, M. S. Strano, E. H. Haroz, K. L. Rialon, P. J. Boul, W. H. Noon, C. Kittrell, J. Ma, R. H. Hauge, R. B. Weisman, and R. E. Smalley, "Band Gap Fluorescence from Individual Single-Walled Carbon Nanotubes", *Science* **297**(5581), 593–596, 2002.

[62] X. Lu and Z. Chen, "Curved Pi-Conjugation, Aromaticity, and the Related Chemistry of Small Fullerenes (<C_{60}) and Single-Walled Carbon Nanotubes", *Chemical Reviews* **105**(10), 3643–3696, 2005.

[63] D. Tasis, N. Tagmatarchis, A. Bianco, and M. Prato, "Chemistry of Carbon Nanotubes", *Chemical Reviews* **106**(3), 1105–1136, 2006.

[64] J. L. Bahr and J. M. Tour, "Covalent chemistry of single-wall carbon nanotubes", *J. Mater. Chem.* **12**, 1952–1958, 2002.

[65] X. Wang, S. M. Tabakman, and H. Dai, "Atomic Layer Deposition of Metal Oxides on Pristine and Functionalized Graphene", *Journal of the American Chemical Society* **130**(26), 8152–8153, 2008.

[66] R. Materoa, A. Rahtua, M. Ritalaa, M. Leskelä, and T. Sajavaarab, "Effect of water dose on the atomic layer deposition rate of oxide thin films", *Thin Solid Films* **368**(1), 1–7, 2000.

[67] S. Haukka, E. L. Lakomaa, and A. Root, "An IR and NMR study of the chemisorption of titanium tetrachloride on silica", *The Journal of Physical Chemistry* **97**(19), 5085–5094, 1993.

[68] R. L. Puurunen, A. Root, S. Haukka, E. I. Iiskola, M. Lindblad, and A. O. I. Krause, "IR and NMR Study of the Chemisorption of Ammonia on Trimethylaluminum-Modified Silica", *The Journal of Physical Chemistry B* **104**(28), 6599–6609, 2000.

[69] A. S. Cavanagh, C. A. Wilson, A. W. Weimer, and S. M. George, "Atomic layer deposition on gram quantities of multi-walled carbon nanotubes", *Nanotechnology* **20**(25), 255602, 2009.

[70] D. B. Farmer and R. G. Gordon, "Atomic Layer Deposition on Suspended Single-Walled Carbon Nanotubes via Gas-Phase Noncovalent Functionalization", *Nano Letters* **6**(4), 699–703, 2006.

[71] X. Feng, S. Irle, H. Witek, K. Morokuma, R. Vidic, and E. Borguet, "Sensitivity of Ammonia Interaction with Single-Walled Carbon Nanotube Bundles to the Presence of Defect Sites and Functionalities", *Journal of the American Chemical Society* **127**(30), 10533–10538, 2005.

[72] S. Wang, Q. Zhang, D. Yang, P. Sellin, and G. Zhong, "Multi-walled carbon nanotube-based gas sensors for NH_3 detection", *Diamond and Related Materials* **13**(4-8), 1327 – 1332, 2004.

[73] Y.-H. Lin, P.-S. Lee, Y.-C. Hsueh, K.-Y. Pan, C.-C. Kei, M.-H. Chan, J.-M. Wu, T.-P. Perng, and H. C. Shih, "Atomic Layer Deposition of Zinc Oxide on Multiwalled Carbon Nanotubes for UV Photodetector Applications", *Journal of The Electrochemical Society* **158**(2), K24–K27, 2011.

[74] C. N. R. Rao, A. Govindaraj, and B. C. Satishkumar, "Functionalised carbon nanotubes from solutions", *Chem. Commun.* **13**, 1525–1526, 1996.

[75] C. Liu, C.-C. Wang, C.-C. Kei, Y.-C. Hsueh, and T.-P. Perng, "Atomic Layer Deposition of Platinum Nanoparticles on Carbon Nanotubes for Application in Proton-Exchange Membrane Fuel Cells", *Small* **5**(13), 1535–1538, 2009.

[76] W. Xia, C. Jin, S. Kundu, and M. Muhler, "A highly efficient gas-phase route for the oxygen functionalization of carbon nanotubes based on nitric acid vapor", *Carbon* **47**(3), 919 – 922, 2009.

[77] D. B. Mawhinney, V. Naumenko, A. Kuznetsova, J. T. Yates, J. Liu, and R. E. Smalley, "Infrared Spectral Evidence for the Etching of Carbon Nanotubes: Ozone Oxidation at 298 K", *Journal of the American Chemical Society* **122**(10), 2383–2384, 2000.

[78] J. Bult, A. Dameron, S. Pylypenko, C. Engtrakul, C. Bochert, L. Chen, J. Leong, S. Frisco, L. Simpson, H. N. Dinh, and B. Pivovar, "Atomic Layer Deposition of Platinum onto Functionalized Aligned MWNT Arrays for Fuel Cell Application", *ECS Transactions* **33**(1), 89–96, 2010.

[79] H. Bubert, S. Haiber, W. Brandl, G. Marginean, M. Heintze, and V. Brueser, "Characterization of the uppermost layer of plasma-treated carbon nanotubes", *Diamond and Related Materials* **12**(3-7), 811 – 815, 2003. 13th European Conference on Diamond, Diamond-Like Materials, Carbon Nanotubes, Nitrides and Silicon Carbide.

[80] T. Xu, J. Yang, J. Liu, and Q. Fu, "Surface modification of multi-walled carbon nanotubes by O2 plasma", *Applied Surface Science* **253**(22), 8945 – 8951, 2007.

[81] B. Khare, P. Wilhite, B. Tran, E. Teixeira, K. Fresquez, D. N. Mvondo, C. Bauschlicher, and M. Meyyappan, "Functionalization of Carbon Nanotubes via Nitrogen Glow Discharge", *The Journal of Physical Chemistry B* **109**(49), 23466–23472, 2005.

[82] Y. H. Yan, M. B. Chan-Park, Q. Zhou, C. M. Li, and C. Y. Yue, "Functionalization of carbon nanotubes by argon plasma-assisted ultraviolet grafting", *Applied Physics Letters* **87**(21), 213101, 2005.

[83] A. Felten, C. Bittencourt, J.-F. Colomer, G. V. Tendeloo, and J.-J. Pireaux, "Nucleation of metal clusters on plasma treated multi wall carbon nanotubes", *Carbon* **45**(1), 110 – 116, 2007.

[84] K. S. Ahn, J. S. Kim, C. O. Kim, and J. P. Hong, "Non-reactive rf treatment of multiwall carbon nanotube with inert argon plasma for enhanced field emission", *Carbon* **41**(13), 2481 – 2485, 2003.

[85] C. Hossbach, S. Teichert, J. Thomas, L. Wilde, H. Wojcik, D. Schmidt, B. Adolphi, M. Bertram, U. Mühle, M. Albert, S. Menzel, B. Hintze, and J. W. Bartha, "Properties of Plasma-Enhanced Atomic Layer Deposition-Grown Tantalum Carbonitride Thin Films", *Journal of The Electrochemical Society* **156**(11), H852–H859, 2009.

[86] L. Qingwen, Y. Hao, Y. Yinchun, Z. Jin, and L. Zhongfan, "Defect Location of Individual Single-Walled Carbon Nanotubes with a Thermal Oxidation Strategy", *The Journal of Physical Chemistry B* **106**(43), 11085–11088, 2002.

[87] S. Nagasawa, M. Yudasaka, K. Hirahara, T. Ichihashi, and S. Iijima, "Effect of oxidation on single-wall carbon nanotubes", *Chemical Physics Letters* **328**(4-6), 374 – 380, 2000.

[88] I. W. Chiang, B. E. Brinson, R. E. Smalley, J. L. Margrave, and R. H. Hauge, "Purification and Characterization of Single-Wall Carbon Nanotubes", *The Journal of Physical Chemistry B* **105**(6), 1157–1161, 2001.

[89] J. L. Zimmerman, R. K. Bradley, C. B. Huffman, R. H. Hauge, and J. L. Margrave, "Gas-Phase Purification of Single-Wall Carbon Nanotubes", *Chemistry of Materials* **12**(5), 1361–1366, 2000.

[90] A. M. Da Silva, G. M. A. Junqueira, C. P. A. Anconi, and H. F. Dos Santos, "New Insights on Chemical Oxidation of Single-Wall Carbon Nanotubes: A Theoretical Study", *The Journal of Physical Chemistry C* **113**(23), 10079–10084, 2009.

[91] E. Mickelson, C. Huffman, A. Rinzler, R. Smalley, R. Hauge, and J. Margrave, "Fluorination of single-wall carbon nanotubes", *Chemical Physics Letters* **296**(1-2), 188–194, 1998.

[92] E. Unger, M. Liebau, G. Duesberg, A. Graham, F. Kreupl, R. Seidel, and W. Hoenlein, "Fluorination of carbon nanotubes with xenon difluoride", *Chemical Physics Letters* **399**(1-3), 280–283, 2004.

[93] M. Dresselhaus, G. Dresselhaus, R. Saito, and A. Jorio, "Raman spectroscopy of carbon nanotubes", *Physics Reports* **409**(2), 47 – 99, 2005.

[94] M. Chhowalla, K. B. K. Teo, C. Ducati, N. L. Rupesinghe, G. A. J. Amaratunga, A. C. Ferrari, D. Roy, J. Robertson, and W. I. Milne, "Growth process conditions of vertically aligned carbon nanotubes using plasma enhanced chemical vapor deposition", *Journal of Applied Physics* **90**(10), 5308–5317, 2001.

[95] F. Tuinstra and J. L. Koenig, "Raman Spectrum of Graphite", *The journal of chemical physics* **53**(3), 1126–1130, 1970.

[96] M. S. Dresselhaus and P. C. Eklund, "Phonons in carbon nanotubes", *Advances in Physics* **49**(6), 705–814, 2000.

[97] Y. Xuan, Y. Q. Wu, T. Shen, M. Qi, M. A. Capano, J. A. Cooper, and P. D. Ye, "Atomic-layer-deposited nanostructures for graphene-based nanoelectronics", *Applied Physics Letters* **92**(1), 013101, 2008.

[98] Rogel-Hernandez, E. Alonso-Nunez, G. Camarena, J. Espinoza-Gomez, H. Aguirre, G. Paraguay-Delgado, and F. R. Somanathan, "Side-wall functionalization of multi-walled carbon nanotubes with t-butyl diazoacetate", *Journal of the Mexican Chemical Society* **55**(1), 7–10, 2011.

[99] W. F. Egelhoff and G. G. Tibbetts, "Growth of copper, nickel, and palladium films on graphite and amorphous carbon", *Phys. Rev. B* **19**, 5028–5035, May 1979.

[100] P. M. Ajayan, T. W. Ebbesen, T. Ichihashi, S. Iijima, K. Tanigaki, and H. Hiura, "Opening carbon nanotubes with oxygen and implications for filling", *Nature* **362**, 522–525, 1993.

[101] P. W. Atkins and J. A. Beran, *Chemie: einfach alles*, ch. 17- Elektrochmie und Thermodynamik, 672–681. VCH Verlagsgesellschaft GmbH, Weinheim, 1996.

[102] C. de Frein and A. R. Barron., "Thermogravimetric Analysis of Single Walled Carbon Nanotube. 13/10/2011 (`http://cnx.org/content/m22972/1.2/`)".

[103] F. A. Abuilaiwi, T. Laoui, M. Al-Harthi, and M. A. Atieh, "Modification and functionalization of multiwalled carbon nanotube (MWCNT) via Fischer esterification", *The Arabian Journal for Science and Engineering, Volume 35, Number 1C* **35**, 37–48, 2010.

[104] C. Gao, H. He, L. Zhou, X. Zheng, and Y. Zhang, "Scalable Functional Group Engineering of Carbon Nanotubes by Improved One-Step Nitrene Chemistry", *Chemistry of Materials* **21**(2), 360–370, 2009.

[105] M. Balkanski, M. Nusimovici, and J. Reydellet, "First order Raman spectrum of Cu2O", *Solid State Communications* **7**(11), 815 – 818, 1969.

[106] S. Guha, D. Peebles, and J. Terence Wieting, "Raman and infrared studies of cupric oxide", *Bulletin of Materials Science* **14**, 539–543, 1991.

[107] J. Elam, C. Nelson, R. Grubbs, and S. George, "Nucleation and growth during tungsten atomic layer deposition on SiO2 surfaces", *Thin Solid Films* **386**(1), 41 – 52, 2001.

[108] D. Mann, A. Javey, J. Kong, Q. Wang, and H. Dai, "Ballistic Transport in Metallic Nanotubes with Reliable Pd Ohmic Contacts", *Nano Letters* **3**(11), 1541–1544, 2003.

List of Figures

List of Tables

Acknowledgments

I would like to express thanks to all the people working at the Fraunhofer ENAS, the Center for Microtechnologies (ZfM) and the Institute of Physics of the TU Chemnitz who contributed in some way to this thesis:

Prof. Dr. Stefan E. Schulz and Prof. Dr. Michael Hietschold for assuming the role as examiner;

Dr. Thomas Waechtler for supervision during this thesis;

Steve Mueller for his practical guidance;

Dr. Sascha Hermann and Holger Fiedler for providing CNT samples and for helpful discussions;

Iris Hoebelt and Cornelia Kowol for the introductory training for the SEM and EDX;

Dr. Raul David Rodriguez and Alexander Villabona for Raman spectroscopy;

Andrea Sendzik and Dr. Steffen Schulze for TEM analyses;

Martin Schmeißer, Jan Sommer and Andreas Zienert for discussions and hints;

Dr. Joerg Schuster and Dr. Eckart Fromm for giving me the idea to perform my bachelor thesis at the Fraunhofer ENAS;

the BAföG agency Chemnitz for providing the financial means during my studies;

my parents, Andrea and Gunter Melzer for their never ending support;

and last but not least Jessica for the very special person she is.

Marcel Melzer
October 2011